Exploring the conformation of mixt *cis-trans* α,β-oligopeptoids: A joint experimental and computational study

G. Dumonteil,[a] N. Bhattacharjee,[b,c] G. Angelici,[a] O. Roy,[a] S. Faure,[a] L. Jouffret,[a] F. Jolibois,*[b] L. Perrin,*[c] and C. Taillefumier*[a]

[a] Université Clermont Auvergne, CNRS, SIGMA Clermont, ICCF, F-63000 Clermont-Ferrand, France

[b] Université de Toulouse-INSA-UPS, LPCNO, CNRS UMR 5215, 135 av. Rangueil, F-31077, Toulouse, France

[c] Université de Lyon, Université Claude Bernard Lyon 1, CPE Lyon, INSA Lyon, ICBMS, CNRS UMR 5246, Equipe ITEMM, Bât. Curien, 43 Bd. du 11 Novembre 1918, 69622 Villeurbanne, France

Abstract

The synthesis and conformational preferences of a set of new synthetic foldamers that combine both the α,β-peptoid backbone and side chains that alternately promote *cis*- and *trans*-amide bond geometries have been achieved and addressed jointly by experiment and molecular modeling. Four sequence patterns were thus designed and referred as *cis*-α-*trans*-β, *trans*-α-*cis*-β, *cis*-β-*trans*-α, and *trans*-β-*cis*-α. α- and β*Nt*Bu monomers were used to enforce *cis*-amide bond geometries and α- and β*N*Ph monomers to promote *trans*-amides. NOESY and molecular modeling reveal that the *trans*-α-*cis*-β and *cis*-β-*trans*-α tetramers show similar pattern of intramolecular weak interactions. The same holds for the *cis*-α-*trans*-β and *trans*-β-*cis*-α tetramers but the interactions are different in nature than those identified in the *trans*-α-*cis*-β based oligomers. Interestingly, the *trans*-α-*cis*-β peptoid architecture allows establishing a larger amount of structure-stabilizing intramolecular interactions.

Introduction

In the past two decades, there has been considerable interest in the construction of synthetic oligomers that are capable of adopting a three-dimensional conformational preference, with the ultimate aim of establishing a close relationship between conformation, properties and functions.[1] The term foldamer was proposed by Gellman to designate "polymers with a strong tendency to adopt a specific compact conformation"[2] and Moore added the notion of structures being "stabilized by a collection of non-covalent interactions between nonadjacent monomer units".[3] In this context a huge number of bioinspired[4] and abiotic foldamers[5] whose skeleton do not resemble those of biopolymers have been constructed and studied. The chemical linkage between the monomers can also be varied expanding backbone chemical diversity and playing a major role on the whole conformation. Native amide bonds are by far the most widely used linkages in foldamer chemistry, not only for its ease of formation, but also for conformational considerations. The amide plane constrains locally the accessible conformational space in addition to its role in intramolecular stabilizing hydrogen bonding. Secondary amides of peptide strands or foldamer structures preferentially exist in solution in the *trans* form, which is energetically most favorable. In peptides, the *cis* amide conformation is mainly observed in proline-rich peptides and *N*-methylated peptides, notably cyclic peptides. There is a special class of artificial oligoamides, namely peptoids where the amides can populate both the *cis* and *trans* conformations. Peptoids are glycine oligoamides with pendant side chains attached on the amide nitrogen atoms.[6] Peptoids are thus characterized by tertiary amide bonds (*N,N*-disubstituted amides) which are prone to *cis-trans* amide isomerism.[7] We are now at a point where it is possible to control the conformation of every peptoid amide bonds within a sequence. This is a formidable opportunity to expand structural diversity of peptoid backbones and foldamers. Oligoamides with an alternating *cis-trans*

amide sequences are very scarce. The alternating *cis-trans* conformation has been observed for oligoprolines with *L/D* alternating configurations.[8] The 4-aminopyroglutamic acids (aPy) have been used as dipeptide mimics with an internal amide linkage locked in the *cis* conformation.[9] The X–ray structure of a trimer of the aPy building block showed a unique, alternating *cis-trans* sequence of amide bonds. In the peptoid field, the Blackwell group has taken advantage of the strong rotameric preference induced by aryl and α-chiral aromatic naphthylethyl (1npe) side chains to construct peptoid oligomers with a succession of *cis* and *trans* main-chain amides. A stable ribbon-like structure was thus revealed by NMR and X–ray crystal analysis.[10] A new and unique peptoid secondary structure referred as "η-helix" was also demonstrated by both alternation of *cis-* and *trans*-promoting side chains and alternation of side chain configuration.[11] The X–ray structure of a number of constrained cyclic peptoids also revealed repetition of the *cis-trans* sequence pattern.[12] Our group has recently described a new peptoid backbone comprising of both α- and β-peptoid monomers in alternation.[13] Herein, we explore the possibility of alternating both α and β monomers and *cis* and *trans* amide main chains within the sequences. α- and β-*Nt*Bu monomers were used for enforcing *cis*-amides and α- and β-*N*Ph monomers for *trans*-amides.[14] Hence, we designed four novel peptoid architectures comprising the α,β backbone and alternating *cis-trans* amides. In this study, we present their synthesis, full NMR analysis and computational study at the tetramer length (compounds **6**, **12**, **19** and **27** in Figure 1).
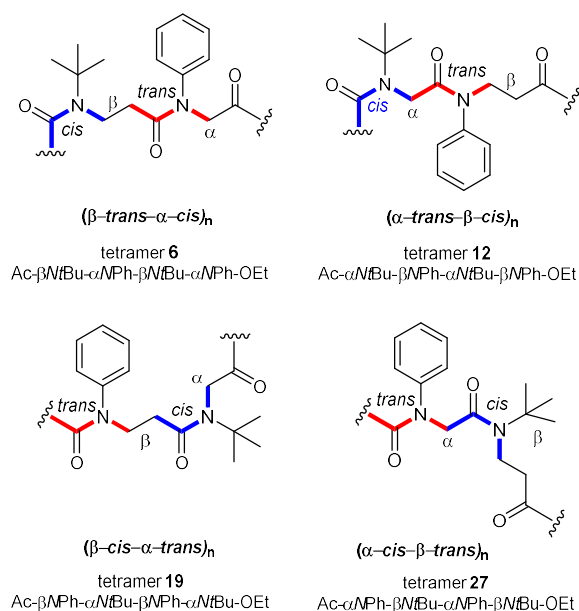
Figure 1. Peptoid architectures based on the alternating α,β-peptoid backbone and alternation of *cis* and *trans* amide bond geometries. CHANGE LABELS IN CDX

Results

Peptoids oligomers are basically more flexible than many other oligoamide-based foldamers due to their inability to establish intramolecular backbone hydrogen-bond networks, achirality of their backbone and equilibria between the *cis* and *trans* tertiary amide conformations. The latter should however be considered as an advantage since it allows exploring a greater conformational space. A great body of work enabled identifying requirements for peptoid chain folding into discrete structures. Hence, α-peptoids composed of *N*Cα-chiral aromatic side chains or bulky side chains fold preferentially into the PolyProline-type I helical structure (PPI) with all the amides in *cis*,[15] whereas *N*-aryl peptoids resemble the Polyproline-type II helix, with the amides in *trans*.[16] It should be noted, however, that with the exception of cyclic peptoids, the number of high-resolution structures is still scarce. This is for a large part attributable to an imperfect control of the amide geometry, giving rise to a substantial conformational heterogeneity. A small number of side chains have been recently designed to

impose tighter control over the amide geometry through steric and stereoelectronic effects. One of the most effective way to induce the *cis* conformation is the α-chiral aromatic (*S*)-1-(1-naphthyl)ethyl (s1npe) group, as shown in peptoid model systems and homooligomers that contain exclusively *cis* amide bonds above the tetramer length.[15d] Other such side chains are the triazolium[17] and *tert*-butyl (*t*Bu)[18] which strongly favor *cis* peptoid amides predominantly based on electronic and steric effects, respectively. The *tert*-butyl group even allows a complete locking of peptoid amides in *cis*, independently of the solvent. Despite the achirality of *t*Bu groups, it was even shown that weak non-covalent interactions, including *t*Bu⋯*t*Bu dispersive interactions help promote helix folding.[18] The *trans* peptoid amide conformation, on the other hand, is mainly favored by the use *N*-aryl side chains, with *cis/trans* ratios ≥ 95:5. We now report on new peptoid platforms design that combines the α,β-backbone and *cis* and *trans* amides in alternation. Four sequence patterns were thus devised from the above-mentioned structural elements: *cis*-α-*trans*-β, *trans*-α-*cis*-β, *cis*-β-*trans*-α, and *trans*-β-*cis*-α. The corresponding compounds were synthesized at the tetramer length (compounds **6**, **12**, **19**, and **27**) with *t*Bu side chains to impose *cis* peptoid amide geometries and phenyl (Ph) side chain for the *trans* conformation.

Synthesis of tetramer 6 (Ac-β*Nt*Bu-α*N*Ph-β*Nt*Bu-α*N*Ph-OEt). α-Peptoids are most often synthesized in high yield and good purity by the solid-phase submonomer protocol described by Zuckermann et al.[19] A solid-phase submonomer approach has been adapted to the synthesis of β-peptoids[20] but efficacy of the two-steps iterative process (acylation with acryloyl chloride followed by aza-Michael addition of primary amines) has been shown to be limited by the second step of the iteration. As our goal was to make short oligomers (4-mers), but also and more importantly due to the deactivated character of aryl amines and the presence of sterically demanding *t*Bu groups within the sequences, we decided to synthesize

peptoid oligomers in solution. The initial general synthetic strategy involving the submonomer synthesis of *N*-to-*C* α,β- and β,α-dimeric building blocks, and their subsequent coupling to form tetramers was considered the most straightforward. We also anticipated that the development of a fragment-based coupling strategy would be suitable for the synthesis of longer oligomers. This strategy was first assessed for the synthesis of tetramer **6** *trans*-β-*cis*-α) (Scheme 1). The synthesis began by treatment of ethyl bromoacetate with 2 equivalents of aniline in chloroform to yield the desired peptoid monomer **1** in modest yield. The next residue (*Nt*Bu β-alanine) was constructed by the two-step submonomer approach including acylation with acryloyl chloride in the presence of triethylamine in THF (**2**, 77% yield), and aza-Michael addition of *tert*-butylamine on the formed acrylamide at 60 °C in ethanol (93% yield). The formed dimer **3** represents the amine dimeric building block of the forthcoming peptide coupling reaction. Therefore, half of the material was kept unchanged and the other half was end-capped by an acetyl group before saponification of the ethyl ester to give the dimer acid **5**, ready for the coupling with **3**. Peptide coupling of peptoid segments substituted by a sterically hindered *tert*-butyl group at the *N*-terminus is very challenging as shown by us recently. Taking advantage of our experience, we first examined the use of pentafluorophenyl diphenylphosphinate (FDPP) and pentafluorophenyl trifluoroacetate, two reagents which allow activation of the acid partner as a pentafluorophenyl ester. Among all the peptide coupling techniques tested, only these reagents have allowed us to synthesize *Nt*Bu α-peptoids with up to 15 residues.[18] Surprisingly, these reagents failed to provide tetramer **6**. We then tested for the first time the Mukaiyama reagent (2-chloro-1-methylpyridinium iodide: CMPI) in the presence of triethylamine, yielding the expected tetramer **6** in 53% yield after several optimization reactions.

Scheme 1. Synthesis of tetramer **6**
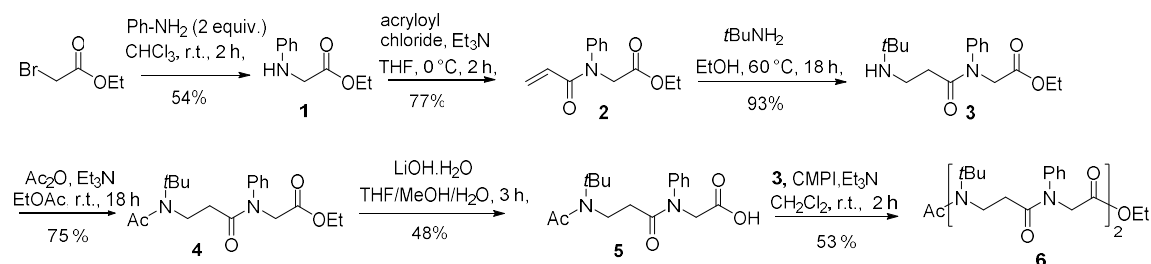
Synthesis of tetramer 12 (Ac-α*Nt*Bu-β*N*Ph-α*Nt*Bu-β*N*Ph-OEt). The same general synthetic approach was applied to the synthesis of tetramer **12** (*trans*-α-*cis*-β) (Scheme 2), *via* the submonomer synthesis of a dimer (**9**), of which a part was converted into the acid partner (**11**) and a final coupling using the Mukaiyama reagent to give tetramer **12**. The difference between compounds **6** and **12** is the inversion between the α- and β-residues. Thus, the synthesis of **12** started with the preparation of the β*N*Ph monomer **7** by addition of aniline onto ethyl acrylate in protic solvents at 100 °C following a described procedure.[21] Elongation consisted in a bromoacetylation reaction and displacement of the bromine with *tert*-butylamine to give dimer **9**.
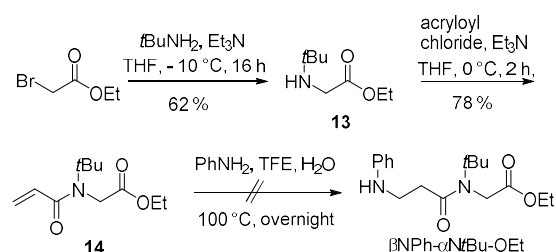
Scheme 2. Synthesis of tetramer **12**
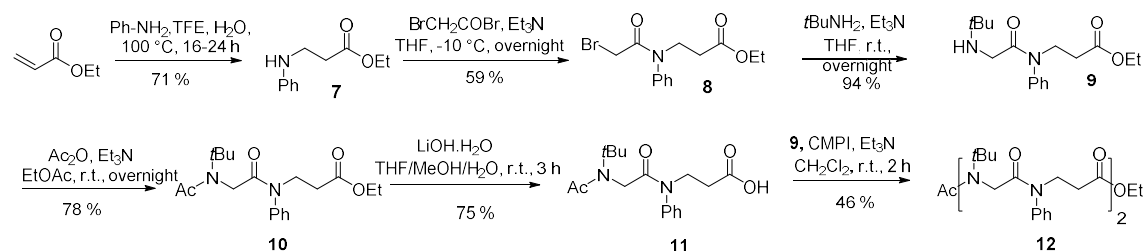
Synthesis of tetramer 19 (Ac-β*N*Ph-α*Nt*Bu-β*N*Ph-α*Nt*Bu-OEt). Afterward we synthesized tetramer **19** using the same general strategy. This involved the synthesis of dimer β*N*Ph-

α*N*tBu-OEt following the same route as for the synthesis of compound **3** but switching the amines in the sequence (Scheme 3). The submonomer compound **14** was thus prepared and treated under the same conditions as for the synthesis of **7** (PhNH$_2$, TFE, H$_2$O, 100°C). Unfortunately, these conditions failed to give the expected dimer β*N*Ph-α*N*tBu-OEt.

Scheme 3. Attempted synthesis of dimer β*N*Ph-α*N*tBu-OEt

Tetramer **19** was finally successfully synthesized by a monomer approach in the *N*-to-*C* direction as shown in Scheme 4. Monomer **7** was first *N*-capped by an acetyl group followed by hydrolysis of the ester to give the acid partner **16**. Coupling of **16** with the amine **13** using the Mukaiyama reagent afforded dimer **17** in 87% yield. Saponification of **17** (77 % yield) and subsequent coupling of the formed acid with **7**, still with the CMPI reagent but in the presence of DMAP[22] afforded trimer **18** (52 % isolated yield), which in turn was hydrolyzed to the corresponding acid and converted by Mukaiyama peptide coupling into the expected tetramer **19**.

Scheme 4. Synthesis of tetramer **19**
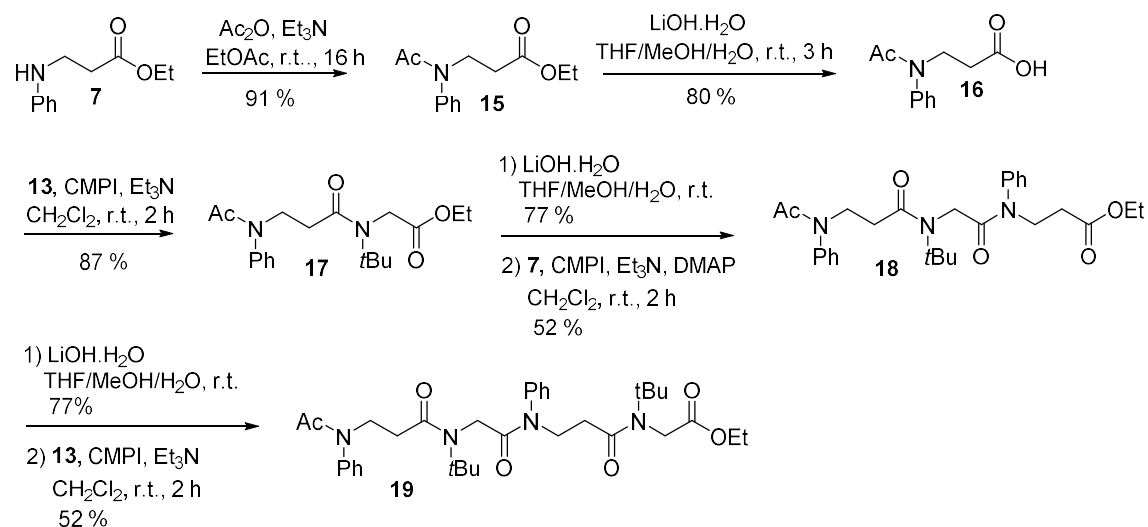
Synthesis of tetramer 27 (Ac-α*N***Ph-β***N***tBu-α***N***Ph-β***N***tBu-OEt).** For the synthesis of tetramer **27**, the initial [2+2] fragment based coupling strategy was also considered, which implied first the submonomer synthesis of dimer amine **22** as shown in Scheme 5. Compound **22** was then converted to the corresponding acid in two steps, consisting in the capping of the *N*-terminal as an acetamide and hydrolysis of the ester function (not shown, see SI for details). The formed acid dimer was then reacted with amine **22** under peptide coupling conditions, with the aim of obtaining the expected tetramer **27**. Three attempts were carried out with the Mukaiyama reagent, changing the additive base (Et₃N, Et₃N/DMAP and DBU). None of them allowed us obtaining tetramer **27**. To address this issue, synthesis of **27** was continued from amine **22** using only submonomer protocols. The synthesis of trimer **24** required acylation of **22** with acryloyl chloride (97% yield) followed by aza-Michael addition of *t*BuNH₂ in 89% yield. From **24**, a last submonomer cycle (bromoacetylation in 34% yield and bromine displacement with aniline in 63% yield) afforded tetramer **26**, which was subsequently acetylated to give the expected compound **27**.

Scheme 5. Synthesis of tetramer **27**
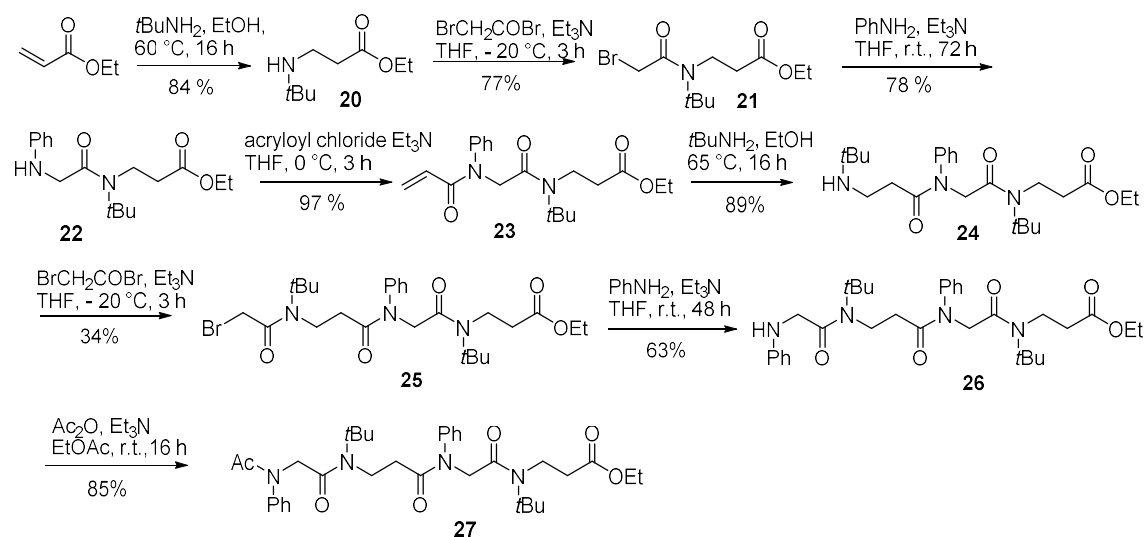
NMR spectroscopic studies. The four synthesized tetramers **6**, **12**, **19**, and **27** were analysed by a combination 2D NMR experiments (^{1}H,^{1}H-COSY, ^{1}H,^{13}C-HMQC, and HMBC) that allowed full assignment of the proton and carbon NMR spectra. Of note is the observation of a single set of resonances for every compound as shown by the ^{1}H-^{13}C HSQC spectra in Figure 2. This is indicative of a full control of the amide bonds geometry by the side chains. 2D-NOESY spectra were acquired to verify geometry of the amides, which, as expected were found *cis* for *Nt*Bu monomers and *trans* for *N*-aryl monomers (ESI S30).

A
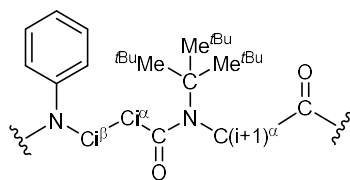
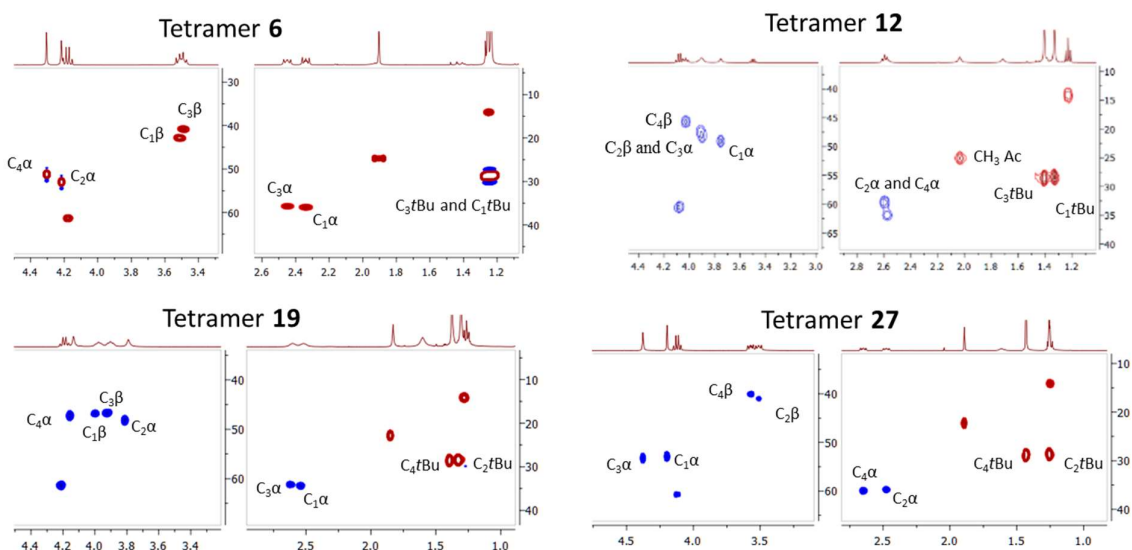
B

Figure 2. ^{1}H-^{13}C HSQC spectra of tetramer **6**, **12**, **19**, and **27** (B). The principle of atom labeling is shown in (A).
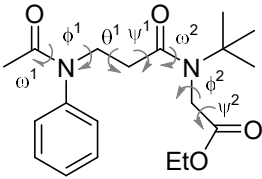
X–ray Crystallography of dimer 17. Single crystals of dimer **17** suitable for X–ray diffraction were grown from slow evaporation of a Et$_2$O solution (Figure 3, Table 1). Dihedral angles of the *Nt*Bu α-monomer at the *C*-terminus match up well with those characterizing peptoid monomers in Polyproline type-I helical secondary structure. Analysis of the β-*N*Ph monomer revealed an extended backbone conformation (θ1 = -172.8, Table 1) as previously observed in the solid-state structure of β-peptoid model compounds.[23]

The crystal structure was analysed for potential non-covalent interactions (Figure 3). The backbone carbonyl groups being oriented roughly perpendicular to each other, implications of n → π*$_{C=O}$ interactions were considered. One potential n → π*$_{C=O}$ interaction was detected between the carbonyl oxygen atom of the ester and the carbonyl amide of the precedent residue. The carbonyl oxygen atom to carbonyl carbon distance is 3.2 Å, as for an ideal polyproline II helix[24] and the O$_{i+1}$···C'$_i$=O angle is 128°, which is only slightly outside of the 109 ± 10° window for an optimal orbital overlap. Such C=O$_{i+1}$···C'$_i$=O interactions have been observed in a β-peptoid monomer[23] and in an *N*-aryl/*N*s1npe tetramer.[10] The directionality of

11

the interaction is however opposite to that which is prevalent in prolyl peptide models (C=O$_{i-1}$···C'$_i$=O)[25] or revealed in previous X–ray crystallographic studies of peptoids.[16b,26]

Table 1. Dihedral angles in dimer **17**

ω1 (*trans*)	φ1	θ1	ψ1	ω2 (*cis*)	φ2	ψ2
+175.80	-75.6	-172.8	-171.1	+4.9	+81.9	+166.8
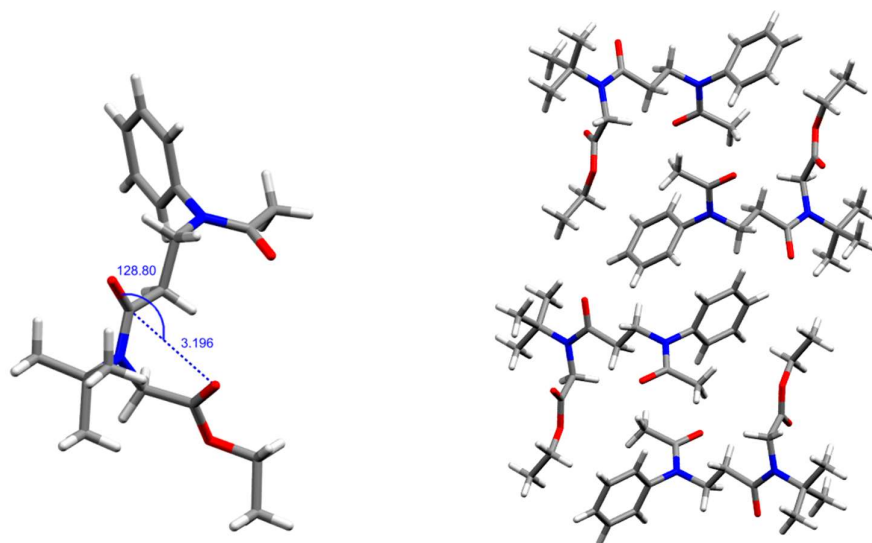
Figure 3. Solid-state structure of dimer **17** (Ac-β*N*Ph-α*Nt*Bu-OEt) determined by X–ray crystallography. (A) single molecule. (B) Packing of **17** within unit cell.

Molecular Dynamics simulations. In order to investigate the folding of oligomers **6**, **12**, **19** and **27**, their dynamical behavior has been probed by classical molecular dynamics simulations. For the 4 types of *cis-trans* peptoid tetramers (**6**, **12**, **19**, and **27**), 50 nanoseconds simulations were performed. During these simulations, and as noticed in our previous study,[18] no change of peptoid ω dihedral angle was observed. As expected, the *t*Bu and Ph side chains

induce *cis* and *trans* peptoid amide bond geometries, respectively.[16a,18] As the folding of peptoids is essentially related to the backbone dihedral angles, the probability distribution of these angles has been analyzed for each trajectory and plotted in 1D and in 2D Ramachandran maps as indicated in Figures S1 to S4. In this study, all initial structures display positive values of φ by construction. The mirror image that would display all negative values of φ would behave similarly and has not been considered.

From Table 2 that gather the different angles combinations, it appears that tetramers **12** and **19** display similar conformational features. The same conclusion can be drawn for tetramers **27** and **6**. As a consequence, regarding the Ramachadran maps provided in ESI and the associated remarkable angles summarized in Table 2, general conformational trends can be highlighted. It appears that the nature of the side chain (ie *t*Bu vs Ph) influences the value of the ϕ angle. The *t*Bu group, that induces a *cis* amide conformation, also constraints the φ angle value that remains unchanged during the simulation time as previously shown by us for α*Nt*Bu oligopeptoids.[18] In contrast, the phenyl group, that induces a *trans* amide conformation, also allows more flexibility and fluxionality of the residue with a larger range of accessible φ angle values. In addition, a second constraint is imposed by the α or β nature of the peptoid residue. This parameter specifically influences the value of the ψ angle. As expected, α peptoid residues are less flexible and induce a narrower range of ψ angle values than β residues.

Considering all these features, and in accordance with Ramachandran maps, each of the four residue involves in the tetramers under study has different conformational behaviors. Tetramers **12** and **19** that contain α*Nt*Bu residue are characterized by a (ψ,φ) couple of angles that remains equal to (+170, +90). In the case of tetramers **6** and **27** that comprise β*Nt*Bu moiety, this combination of angles takes predominantly the same values (180, +90). However, for **6** and **27**, two other regions of the Ramachandran plots start to be populated. These

regions that spreads toward the value +90 and -90 degrees correspond to the modification of ψ angle distribution allowed by the β character of the residue. If tetramers **6** and **27** that include a αNPh residue are now considered, the main population of the (ψ,φ) couple of angles is at (180, +90), as for $\alpha N t$Bu residue, but two additional regions are also populated. One corresponds to (180, -90) and is the symmetric of the previous mainly populated area, while the second is characterized by a new set of angles (+70, -160) with its symmetric counterpart (-70, 160) that is slightly populated for the final fourth residue of tetramer **6**. Finally, the more "flexible" residue appears to be βNPh that is included in tetramers **12** and **19**. For this residue, the associated Ramachandran plots exhibit a larger number of populated regions. However, depending on the location of this residue within the tetramer, these regions are not equally populated. Whilst residue 4 of tetramer **12** almost populates equally the (ψ,φ) regions (180, ±90), (+90, ±90), (-90, ±90) for symmetric reasons, these population are less pronounced for the other βNPh residue locations. For residue 1 in tetramer **19**, this population is less homogeneous, but 6 regions are still distinguishable in the (ψ,φ) Ramachadran maps. This large amount of conformations that are explored by these two residues can be explained by the fact that there are terminus residues in the foldamer. In the case of "internal" βNPh residue, the population of these regions is more heterogeneous. Residue 3 of **19** clearly shows a preference for the (+100,+90) region, even if (-170, ±90) and (-90, -90) regions remain slightly populated. The scenario is completely different for residue 2 of tetramer **12**. In this case, the only region of the (ψ,φ) Ramachadran plot that is populated correspond only to (+90,-100). This can be correlated to the value of the θ angle that characterizes β peptoid units and that has not yet been taken into account. Indeed, for all βNtBu residues, the θ angle is equal to 180°. For βNPh moiety, this angle is also mostly equal to 180°, except for residue 2 in tetramer **12** for which this angle take the value of +60°. The (ψ, φ, θ) combination of (+90, -100, +60) seems to be also slightly populated for some other βNPh moiety but in a lesser

14

extent. Longer simulation or Replica exchange molecular dynamics would be necessary to be performed in order to improve our ergodicity and to improve the population of each region that have been highlighted. However 150ns of simulation for such tetramers already allows to highlight conformational trends that matches experimental spectroscopic analysis as discussed below. In addition, it is worth to note that concerning peptoid **19**, simulated structural parameters are in agreement with the experimental values determined by X–ray crystallography (see Table 2).

Table 2. Conformational trends of tetramers **6**, **12**, **19** and **27** given by averaged simulated and experimentally determined dihedral angles. Dihedral angles definition: ω [$C_\alpha(i\text{-}1)$; $C(i\text{-}1)$; N; C_α or C_β], $\varphi_{(\alpha\text{-monomer})}$ [$C(i\text{-}1)$; N; C_α; C], $\varphi_{(\beta\text{-monomer})}$ [$C(i\text{-}1)$; N; C_β; C_α] $\psi_{(\alpha\text{-monomer})}$ [N; C_α; C; $N(i\text{+}1)$], $\psi_{(\beta\text{-monomer})}$ [C_β; C_α; C; $N(i\text{+}1)$]. Values in bold indicates preferential conformation(s).

Ac-α*Nt*Bu-β*N*Ph-α*Nt*Bu-β*N*Ph-OEt (**12**)				
residue id.	ω	ϕ	ψ	θ
α*Nt*Bu (1)	-10	**+90 ±10**	**+170 ±20**	-
α*Nt*Bu (3)	-10	**+90 ±10**	**+170 ±20**	-
β*N*Ph (2)	180	**−100 ±10** +85 ±10	**+90 ±10** +90 ±10	**+60 ±10** +60 ±10
β*N*Ph (4)	180	**+90 ±10** -90 ±10 ± 90 ±10	**180 ±10** 180 ±10 ± 90 ±10	**180 ±10** 180 ±10 180 ±10

Ac-βNPh-αNtBu-βNPh-αNtBu-OEt (**19**)				
residue id.	ω	φ	ψ	θ
αNtBu (2)	-10	**+90 ±10**	**+170 ±20**	-
αNtBu (4)	-10	**+90 ±10**	**+170 ±20**	-
17 (X–ray)	**+5**	**+82**	**+167**	
βNPh (1)	180	**± 90 ±10** ± 90 ±10	**-170 ± 20** +100 ±20	**180 ±10** 180 ±10
βNPh (3)	180	**+90 ±10** ±90 ±10 -90 ±10	**+100 ± 20** -170 ±20 +100 ±20	**-170 ±10** -170 ±10 -170 ±10
17 (X–ray)	**+176**	**-76**	**-171**	**-172**

Ac-αNPh-βNtBu-αNPh-βNtBu-OEt (**27**)				
residue id.	ω	φ	ψ	θ
αNPh (1)	180	**±90 ±20** -160 ±20	**180 ±20** +70 ±20	-
αNPh (3)	180	**±90 ±20** **-160 ±20** +160 ±20	**180 ±20** **+70 ±20** -70 ±20	-
βNtBu (2)	+10	**+90 ±10** **+90 ±10** +90 ±10	**180 ±20** **+90 ±20** -90 ±20	**180 ±10** **180 ±10** 180 ±20

residue id.	ω	φ	ψ	θ
βNtBu (4)	+10	+90 ±10	180 ±20	180 ±10
		+90 ±10	+90 ±20	180 ±20
		+90 ±10	-90 ±20	180 ±20

Ac-βNtBu-αNPh-βNtBu-αNPh-OEt (6)				
residue id.	ω	φ	ψ	θ
αNPh (2)	180	±90 ±20	180 ±20	-
		-160 ±20	+70 ±20	
αNPh (4)	180	±90 ±20	180 ±20	-
		-160 ±20	+70 ±20	
		+160 ±20	-70 ±20	
βNtBu (1)	+10	+90 ±10	180 ±20	180 ±20
		+90 ±10	+90 ±20	+170 ±20
		+90 ±10	-90 ±20	-170 ±20
βNtBu (3)	+10	+90 ±10	180 ±20	180 ±20
		+90 ±10	+90 ±20	+170 ±20
		+90 ±10	-90 ±20	-170 ±20

Quantum Chemical Calculations.

Energetics and conformations. The energetics associated to the φ angle rotation of αNPh and βNPh residues has been evaluated in tetramers **6** and **12**, respectively, by means of a relaxed energy potential scan computed at the HF/Ahlrichs-VDZ level for optimizations and refined at the M06-2X/6-311G(d,p) level for energy evaluations. See the Experimental section for details. In both cases, two minima are clearly identified (Figure S5) and dihedral angles corresponding to the most stable conformers match the distribution of the φ angle obtained by

molecular dynamics (see Figures S1 and S4). For both the αNPh and βNPh residues, the most stable conformers are interconnected by low energy transition states (below 6 kcal mol^{-1}). This suggests a similar fluxionality of these two residues regarding the φ torsion angle.

A Ac-βNtBu-αNPh-βNtBu-αNPh-NMe$_2$ (**6'**)

B Ac-αNtBu-βNPh-αNtBu-βNPh-NMe$_2$ (**12'**)

C Ac-βNPh-αNtBu-βNPh-αNtBu-NMe$_2$ (**19'**)

D Ac-αNPh-βNtBu-αNPh-βNtBu-NMe$_2$ (**27'**)
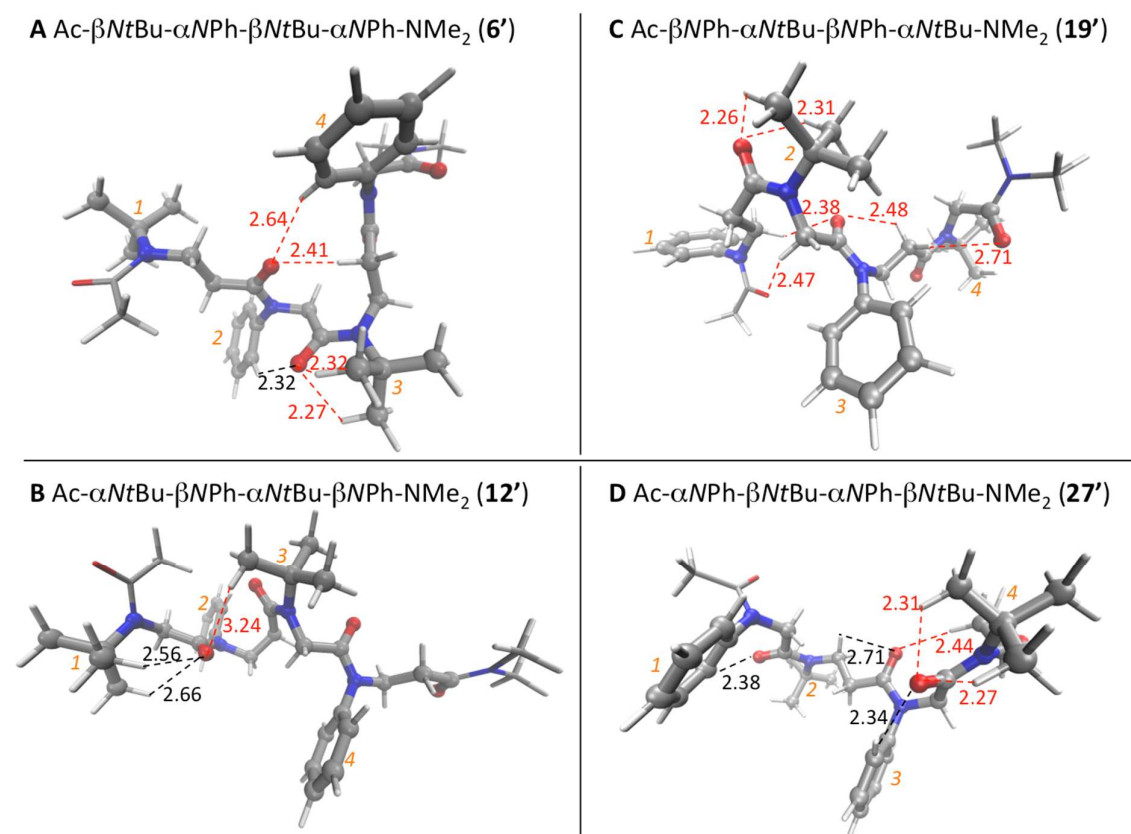
Figure 4. 3D representation of the optimized geometry at the DFT level of tetramers **6**, **12**, **19**, and **27** in which representative key weak (CH$^{...}$O) dispersive interactions are identified by their distances (Å). Intra-residue interactions are displayed in black, inter-residue interactions are displayed in red. Residue index are given in orange. For these calculations, *C*-termini of tetramers have been capped by NMe$_2$ (prime tag) amide group in place of the ester function used experimentally.

From the optimized geometries at the quantum level (Figure 4) and analysis of conformational parameters of each tetramer (Table 2), it appears that two main driving forces are responsible

for the conformational features of tetramers **6**, **12**, **19**, and **27**. One should mention that some interaction types displayed in Figure 4 on structures optimized at the quantum level could differ from those integrated along classical molecular dynamic trajectories. Firstly, intra-residue (Ph-H$^{...}$O=C) hydrogen bondings seem to govern specific conformational properties. In the case of tetramers **6** and **27** for which the phenyl side chains are attached to α-peptoid monomers, this specific interaction is systematically encountered. This can be related to almost identical dihedral angles of the αNPh residues for these two tetramers (Table 2). By contrast, when the phenyl groups are attached to β peptoid residues, the enhanced local flexibility in conjunction with the *trans* character of the peptoid amide bond cannot insure a systematic (Ph-H$^{...}$O=C) hydrogen bond. This is reflected by a greater fluctuation of the ψ torsion angles of βNPh residues of tetramers **12** and **19**. Secondly, the *cis* conformation imposed by the *t*Bu side chains results in systematic weak $(t\text{Bu})^{(i+1)}\text{CH}^{...}\text{O=C}^{(i)}$ interactions[18] independently of the α or β nature of the NtBu monomers. This induces conserved local conformations as reflected by similar dihedral angle for the N-*t*Bu residues of tetramers **12** and **19** on one hand, and tetramers **6** and **27,** on the other (Table 2).

Folding driving forces. In our previous study on αNtBu peptoids oligomers, we have shown that weak dispersive interactions play a significant role to the peptoid folding.[18] One of these contributions is the dispersive backbone $^{(i)}\text{CH}^{...}\text{O=C}^{(i+1)}$ interaction. This interaction has been monitored for all the simulations of each tetramer, the result are plotted in Figure S6. For tetramers **12** and **19** the carbonyl oxygen atoms of βNPh residues ($i+1$) interact with the Cα methylene protons of the precedent NtBu residue (i), and not the vice versa (label blue, Figure 5). Interestingly, interactions implying the carbonyl oxygen of NPh residues are also revealed in compounds **6** and **27**, in this case between the C=O of αNPh ($i+1$) residues and the Cβ methylene protons of βNtBu (i) residues (Figure 5, label green and Figure S7).
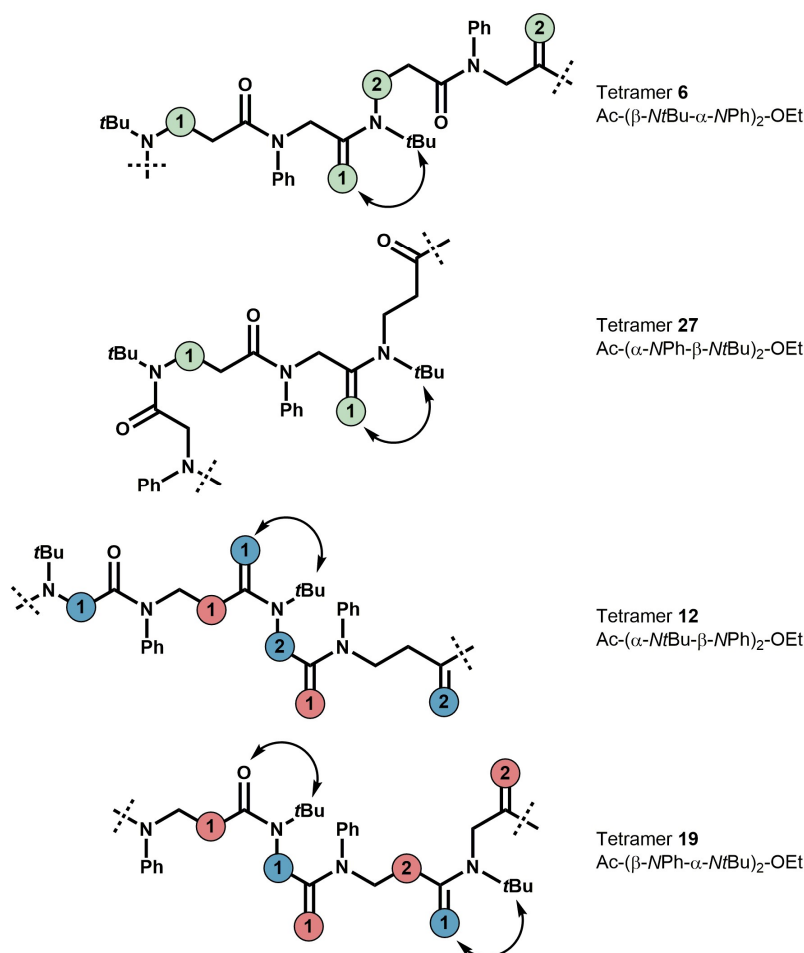
Figure 5. Main chain CH···O=C interactions in tetramers **6**, **12**, **19**, and **27**. Blue (type I), pink (type II), and green (type III) tags refers to $\alpha^{(i)}C_\alpha H \cdots O=C^{(i+1)}$, $\beta^{(i)}C_\alpha H \cdots O=C^{(i+1)}$, and $\beta^{(i)}$ $C_\beta H \cdots O=C^{(i+1)}$ interactions types, respectively. The arrows (type IV) denotes $(t Bu)^{(i+1)}CH$ $\cdots O=C^{(i)}$ interactions. Number labels tag the groups in interactions.

Interestingly, only the C_α methylene groups of β*N*Ph residues (i) show a significant amount of <mark>dispersive</mark> interactions with the CO groups of α*Nt*Bu residues (*i+1*) (Figure 5, pink label and Figure S7). In summary, for the β-residues, the C_α-methylene groups are involved in CH···O=C interactions in case of *N*Ph monomers, whereas the C_β-methylene are involved in case of *Nt*Bu monomers. (CH···O) <mark>dispersive</mark> interactions can also develop between the

backbone carbonyl oxygens and peptoid side chains.[188] Whereas no significant interaction is observed between CO and Ph side chains, the C=O of *N*Ph residues (*i*) interact with the methyl groups of the *Nt*Bu side chains (*i+1*) (Figure S8). No significant difference was found for this interaction with respect to the four different peptoid chains studied in this work.

Aside the interactions that involve the polar backbone carbonyl groups, additional weak interactions can develop between side chains. Recently, we have demonstrated that side chain *t*Bu···*t*Bu interactions help promote helix folding of α-peptoids.[188] In the present case, alternation of *t*Bu and Ph side chains prevents *t*Bu / *t*Bu contact. However, a significant amount of interactions is observed between *t*Bu and Ph side chains (Figure S9). As expected, these interactions are prominent between adjacent residues. However, peptoids that include α*N*Ph residues show a larger amount of interactions than those containing β*N*Ph residues. For tetramer **12**, exclusively, an interaction is pinpointed between the *t*Bu and Ph side chains at the *N*- and *C*-termini, respectively. This proximity is supported by The NOESY spectrum of tetramer **12** (ESI, S33)

Finally, a significant amount of Ph-Ph interactions were observed during the simulations (Figures S10 and illustration in S11). Peptoids with α*N*Ph residues show more interactions than those that comprise β*N*Ph residues. From Figure S10, two patterns of interaction can be highlighted. One traduces a random proximity. The other one traduces a edge-to-face stacking between two Ph groups.

NMR spectra simulation. [1]H and ^{13}C isotropic chemical shifts have been computed for the four tetramers. For that purpose, a set of 500 structures has been extracted from each MD trajectory. Chemical shielding were calculated at the DFT B3LYP[27]/6-31G(*d*,*p*)[28] GIAO level[29] for each structure, and averaged in order to produce simulated NMR spectra. Computed chemical shifts are relative to the theoretical ^{1}H and ^{13}C chemical shielding

computed at the same level of theory.[30] The fit between experimental and theoretical NMR data has been assessed for the four tetramers by means of a linear interpolation. Table 3 summarizes the parameters related to these interpolations together with additional RMSD calculations.

Table 3. Correlation between computed and experimental NMR chemical shifts of tetramers **6**, **12**, **19** and **27**.

Cpd.	**27**	**12**	**19**	**6**
	Ac-(αNPh-$\beta N t$Bu)$_2$-OEt	Ac-($\alpha N t$Bu-βNPh)$_2$-OEt	Ac-(βNPh-$\alpha N t$Bu)$_2$-OEt	Ac-($\beta N t$Bu-αNPh)$_2$-OEt
		^{13}C		
R^2	0.9992	0.9992	0.9993	0.9992
slope	0.92	0.92	0.92	0.92
intercept[a]	5.11	5.03	5.00	5.47
RMSD[a]	5.14	5.21	5.10	5.28
		^{1}H		
R^2	0.9988	0.9981	0.9978	0.9987
slope	1.07	1.05	1.06	1.05
intercept[a]	-0.41	-0.28	-0.30	-0.28
RMSD[a]	0.22	0.20	0.22	0.18

[a] in ppm. R^2, slope and intercept result from a linear interpolation. RMSD: root mean square difference.

For each tetramer, an excellent correlation between computed and experimental ^{1}H and ^{13}C NMR shifts was obtained as illustrated by correlation coefficient higher than 99.78%. The

deviation between computed and ideal slope and y-axis intercept, 1 and 0 respectively, traduces approximations that are inherent to our computational strategy e.g. empirical force field for the structure, solvation models, quantum chemical approximation for the NMR calculations. The quality of these results makes us confident in the relevance of our molecular dynamics simulations. This also raises the confidence regarding the analysis of the molecular conformations generated by molecular dynamic simulations.

Discussion

Synthesis. The initial plan to synthesize the four target tetramers was based on convergent [2+2]-fragment coupling reactions, with the view that this strategy would be very convenient for the preparation of longer oligomers. This strategy was effectively applied for synthesizing tetramers **6** and **12** using the Mukaiyama reagent (2-chloro-1-methylpyridinium iodide, CMPI) as the coupling reagent. These compounds were isolated with average yields of 50%, highlighting the difficulties in coupling terminal *Nt*Bu peptoids amines.[18] In contrast the peptoid fragment coupling strategy was not effective to prepare tetramers **19** and **27**. Regarding the synthesis of tetramer **27**, the coupling of the two dimer blocks Ac-α*N*Ph-β*Nt*Bu-OH and α*N*Ph-β*Nt*Bu-OEt (**22**) failed, likely to the deactivated character of the terminal aryl amine moiety of dimer **22**. The submonomer approach using highly reactive halogenoacyl reagents, bromoacetylbromide and acryloyl chloride for α- and β-monomer synthesis, respectively, was then implemented for synthesizing tetramer **27**. Turning now to the synthesis of tetramer **19**, comprising β*N*Ph and and α*Nt*Bu residues: Synthesis of the required dimer β*N*Ph-α*Nt*Bu-OEt, for subsequent coupling with a dimer acid partner, was not feasible because of the low reactivity of the submonomer acrylamide compound **14** towards the aza-Michael addition of aniline. Fortunately tetramer **19** could be synthesized by a monomer approach in the N-to-C direction, using the Mukaiyama reagent. Synthesis of

tetramers **6**, **12**, **19**, and **27** were thus realized in different ways, involving submonomer, monomer, and fragment-coupling strategies or any combination thereof.

Conformational studies. As the set of structures used to simulate ^{1}H and ^{13}C NMR spectra are extracted from the Molecular Dynamic simulations initially performed to explore the conformation and the dynamics of the four tetramers, the remarkable fit between experimental and computed NMR spectra strongly support both the NMR attribution and the MD simulation protocol. It also validates the parameters and topologies developed for the non-standard α*N*Ph, α*Nt*Bu, β*N*Ph and β*Nt*Bu residues.

A comparative study of the dihedral angles distribution and intramolecular interactions highlights similarities between tetramers **6** Ac-(β*Nt*Bu-α*N*Ph)$_2$-OEt and **27** Ac-(α*N*Ph-β*Nt*Bu)$_2$-OEt on the one hand, and **12** Ac-(α*Nt*Bu-β*N*Ph)$_2$-OEt and **19** Ac-(β*N*Ph-α*Nt*Bu)$_2$-OEt on the other hand (Table 2). For compounds **6** and **27**, analysis of the probability distribution of dihedral angles reveals common trends. For example, the α*N*Ph residues 2 and 3 of tetramers **6** and **27**, respectively − which are positioned internally within the sequences − display a conformation featuring torsion angles around $(\phi,\psi) = (+75°, 180°)$. These values are consistent with those measured in the crystal structure of *N*−aryl peptoid dimers but a deviation is observed from the computationally predicted values $(\phi,\psi) = (+60°, \pm150°)$ for *N*−aryl oligomers.[16a] Regarding now the internal β*Nt*Bu residues 3 (tetramer **6**) and 2 (tetramer **27**), they predominantly populate a conformational state around $(\phi,\psi,\theta) = (+90°, 180°, +175°)$. Interestingly, these torsion angles are very similar to those measured in the crystal structure of a β-peptoid helix with the amide bonds in the *cis*−geometry.[31] Similarly, the α*Nt*Bu residues of tetramers **12** and **19** adopt common conformational features with (ϕ,ψ) torsion angles values at about $(+90°, +170°)$, which are reminiscent of those characterizing polyproline type I helices.[18] Lastly, similarities between the dihedral angles of the β*N*Ph

residues of **12** and **19** are also observed, with essentially two set of values, $(\phi,\psi,\theta) = (\pm 90,$ +100, +180) and $(\phi,\psi,\theta) = (\pm 90, \pm 170, +180)$. This latter set of dihedral angles matchs up well with those determined from the X–ray crystallographic structure of dimer **17** (Ac-(βNPh-$\alpha N t$Bu)$_2$-OEt). With the exception of a θ value around (+60) for residue 2 of tetramer **12**, the θ dihedral angles are systematically observed at about 180°, which means that the $\beta N t$Bu and βNPh residues adopt an extended conformation within the oligomers. Analysis of the intramolecular interactions also revealed similar characteristics between pair of compounds **12**/**19** and **6**/**27**. As highlighted in Figure 5, tetramers **12** and **19** composed of $\alpha N t$Bu and βNPh monomers display $(i,\ i+1)$ inter-residue (CH$^{...}$O) hydrogen bonding involving one backbone methylene atom of the $\alpha N t$Bu (i) residues and the carbonyl oxygen atom of the $(i+1)$ βNPh residues (type I interaction, Figure 5). An additional (CH$^{...}$O) interaction between adjacent residues is identified in **12** and **19**. This involves the backbone Cα methylene protons of βNPh monomers and the C=O of the $(i+1)$ $\alpha N t$Bu residues (type II). Finally, a third interaction between the oxygen atom of the carbonyl groups of the βNPh residues (i) and the methyl protons of the tBu side chains of the $(i+1)$ residues was found omnipresent within **12** and **19** (type IV). Hence, two type I, one type II and two type IV − taking into account the N-terminus acetyl group − interactions participate to the conformational stabilization of tetramer **12**. In tetramer **19**, alternation between the same $\alpha N t$Bu and βNPh residues is maintained. Thereof, one type I, two type II and two type IV interactions are identified. At the tetramer stage, differences in relative conformational stability of **12** and **19** can be expected, but these differences may vanish for longer oligomer length.

In tetramers **6** and **27**, a 4th type of interaction (Cβ–H$\beta^{...}$O=C) is identified between the αNPh carbonyl backbone oxygens and the Cβ methylene protons of $\beta N t$Bu residues (type III, Figure 5). As a result, in tetramer **27**, one type III and two type IV interactions can develop; in

tetramer **6**, two type III and two type IV – taking into account the N-terminus acetyl group – and interactions were pinpointed. The same analysis conducted for tetramers **12** and **19** regarding the length of the oligopeptoids can be transposed to tetramers **6** and **27**. Interestingly, the amount and the nature of interactions differ between the oligopeptoids comprising α*Nt*Bu and β*N*Ph monomers in alternation, on the one hand (exemplified by tetramers **12** and **19**), and those based on α*N*Ph and β*Nt*Bu on the other (exemplified by tetramers **6** and **27**). More backbone inter-residue (CH··O) hydrogen bonding can be established in oligomers based on the α*Nt*Bu-β*N*Ph dimer unit than in oligomers based on the α*N*Ph-β*Nt*Bu one. By contrast, interactions involving only peptoid side chains (*t*Bu/Ph and Ph/Ph H··H contacts) are more numerous for tetramers **6** and **27** (α*N*Ph-β*Nt*Bu-based oligomers) than for **12** and **19** (α*Nt*Bu-β*N*Ph-based oligomers). It therefore appears that in these systems, the more backbone-backbone interactions are present, the less side chain-side chain interactions are found, and *vice-versa*.

Finally, for compounds **12** and **19** on the one hand and for **6** and **27** on the other, similar conformational characteristics have been highlighted by NOESY and molecular dynamic simulations. This suggests that the shift in indexation between analogues **12** and **19**, and **6** and **27**, does not affect the folding of the tetramers. However, the short length of the oligomers limits the number of accessible weak interactions and thus hampers the folding of the peptoid tetramers under study

Conclusion

In this study, we have achieved the synthesis and assessed the conformational preference of a set of new oligopeptoid scaffolds that combine an alternated α,β-backbone with a *cis* and *trans* alternation of the amide links. With this combinatory, four sequence patterns were designed and named *cis*-α-*trans*-β, *trans*-α-*cis*-β, *cis*-β-*trans*-α, and *trans*-β-*cis*-α. The strict

control of the *cis/trans* conformation of the peptoid amide bonds was enabled, respectively, by the use of α and β*Nt*Bu and α and β*N*Ph monomers. The conformation of the four target tetramers was probed by NMR spectroscopy and explored by molecular modeling. Both experimental and theoretical analyses reveal that the *trans*-α-*cis*-β (**12**) and *cis*-β-*trans*-α (**19**) tetramers, comprising both α*Nt*Bu and β*N*Ph monomers, display similar pattern of weak intramolecular interactions. Similarly, the *cis*-α-*trans*-β (**27**) and *trans*-β-*cis*-α (**6**) compounds involving α*N*Ph and β*Nt*Bu residues show similar patterns of weak inter-residues interactions, which are different in nature from those identified in **12** and **19**. Among them, several backbone $^{(i)}$CH$\cdots$O=C$^{(i+1)}$ dispersive interactions between neighboring residues: (i) α*Nt*Bu / β*N*Ph, (ii) (C$_\alpha$H) β*N*Ph / α*Nt*Bu, (iii) (C$_\beta$H) β*Nt*Bu / α*N*Ph; and backbone-side chain $^{(i)}$CH$\cdots$O=C$^{(i-1)}$ interactions: (i) α*Nt*Bu / β*N*Ph, (ii) β*Nt*Bu / α*N*Ph.

Finally, more intramolecular interactions can be established in oligomers constructed from the α*Nt*Bu and β*N*Ph units than from oligomers based on the α*N*Ph and β*Nt*Bu monomers. By contrast with *N*tBu α-oligopeptoids, less intramolecular side chain to side chain interactions can be established in these novel peptoid families. This study also stresses the diversity of weak interactions that can be established within oligopeptoids bearing both aromatic and aliphatic side chains as well as the importance of their collectivity along the sequence to ensure folding. Considering our experience in synthesizing peptoids with *t*Bu side chains and the electronically deactivated character of *N*Ph amines, solution-phase syntheses were conducted in this work. Two tetramers (**12** and **19**) have been constructed from the α*Nt*Bu and β*N*Ph monomers and the two others (**6** and **27**) from the α*N*Ph and β*Nt*Bu monomers. In either case, different synthetic strategies were needed to get the target molecules highlighting expected difficulties arising from the *t*Bu and Ph side chains. From this work, it appears that only tetramers **6** and **12**, prepared from dimers **3** (β*Nt*Bu-α*N*Ph-OEt) and **9** (α*Nt*Bu-β*N*Ph-OEt), could be synthesized following a convergent fragment-based coupling strategy. These

dimer building blocks will serve to construct longer oligomers whose folding will depend on a collection of local interactions that have been detected in the short peptoids. We anticipate that these new systems could serve as suitable platforms to construct high order nanostructures showing various features and applications.

EXPERIMENTAL SECTION

General Information and Materials.

THF, CH_2Cl_2 and MeOH were dried over aluminum oxide via a solvent purification system. EtOAc, CH_2Cl_2, cyclohexane, and MeOH for column chromatography were obtained from commercial sources and were used as received. Et_3N was dried over KOH. All other solvents and chemicals obtained from commercial sources were used as received. Melting points were determined on a Stuart Scientific SMP3 microscope apparatus and are uncorrected. IR spectra were recorded on a Shimadzu FTIR-8400S spectrometer equipped with a Pike Technologies MIRacle™ ATR and ν are expressed in cm^{-1}. NMR spectra were recorded on a 400 MHz Bruker Avance III HD spectrometer or a 500 MHz Bruker AC-500 spectrometer. Chemical shifts are referenced to the residual solvent peak and J values are given in Hz. The following multiplicity abbreviations are used: (s) singlet, (ls) large singlet, (d) doublet, (t) triplet, (q) quartet, (m) multiplet, and (br) broad. Where applicable, assignments were based on COSY, HMBC, HSQC and ^{13}C-experiments. TLC was performed on Merck TLC aluminum sheets, silicagel 60, F_{254}. Progression of reactions was, when applicable, followed by NMR and/or TLC. Visualizing of spots was effected with UV-light and/or vanillin in $EtOH/H_2SO_4$. Flash chromatography was performed with Merck silica gel 60, 40-63 μm. HRMS was recorded on a Micromass Q-Tof Micro (3000 V) apparatus or a Q Exactive Quadrupole-Orbitrap Mass Spectrometer. LC-MS was recorded a Q Exactive Quadrupole-Orbitrap Mass Spectrometer coupled to a UPLC Ultimate 3000 (Kinetex EVO C18; 1.7μm; 100mm x 2.1mm column with

a flow rate of 0.45 mL min^{-1} with the following gradient: a linear gradient of solvent B from 5% to 95% over 7.5 min (solvent A = H$_2$O + 0.1% formic acid, solvent B = acetonitrile + 0.1% formic acid) equipped with a DAD UV/VIS 3000 RS detector. HPLC analysis was performed on a Dionex instrument equipped with an Uptisphere® (ODB, 5 μm, 120 Å, 4.6×250 mm) and a Dionex UVD 340 detector. X-ray data were collected at 100K with an Oxford Diffraction Xcalibur 2 diffractometer equipped with a copper microsource (λ = 1.5418 Å).

General Procedure A: Acetylation of the N-terminal amine of peptoids using Ac$_2$O.

To a solution of peptoid (1 equiv.) and Et$_3$N (4 equiv.) in EtOAc (0.2 M) was added Ac$_2$O (8 equiv.). After stirring overnight at room temperature, the precipitate was filtered off and rinsed with EtOAc. The filtrate was then concentrated under reduced pressure, and purified by column chromatography on silica gel.

General Procedure B: Saponification using LiOH.H$_2$O.

To a solution of peptoid (1 equiv.) in a mixture THF/MeOH/H$_2$O (4/1/1, v/v) was added LiOH.H$_2$O (3 equiv.). After stirring for 3 h at room temperature, the mixture was acidified with HCl 1N and extracted with EtOAc. The organic layer was dried over Na$_2$SO$_4$ and then concentrated *in vacuo*. The crude peptoid acid was used in the peptide-type coupling reaction without further purification.

General Procedure C: Coupling reaction with the Mukaiyama reagent (2-chloromethylpyridinium iodide).

To a solution of the peptoid acid (1.0 equiv.) in CH$_2$Cl$_2$ (0.03 M), was added the Mukaiyama reagent (1.5 equiv.). The mixture was stirred at room temperature for 1 h then a mixture of peptoid amine (1.0 equiv.) and Et$_3$N (3.0 equiv.) in solution in CH$_2$Cl$_2$ was added dropwise. After stirring for 2 h at room temperature, the resulting mixture was diluted with EtOAc and

washed with water. The resulting organic layer was dried over Na_2SO_4 and concentrated under reduced pressure.

General Procedure D : Coupling reaction with the Mukaiyama reagent and DMAP.

To a solution of the peptoid acid (1.0 equiv.) in CH_2Cl_2 (0.03 M), was added the peptoid amine (1.0 equiv.), Et_3N (6.0 equiv.), DMAP (1.0 equiv.) and the Mukaiyama reagent (1.5 equiv.). After stirring for 3 h at room temperature, the resulting mixture was diluted with EtOAc and washed with water. The organic layer was dried over Na_2SO_4 and concentrated under reduced pressure.

Ethyl 2-[3-(*N-tert*-butylacetamido)-*N*-phenylpropanamido]acetate (4).

To a solution of aniline (3.21 mL, 23.95 mmol,) in $CHCl_3$ (10 mL), was added ethyl bromoacetate (1.33 mL, 11.98 mmol). The reaction was stirred at room temperature for 2 h then concentrated under reduced pressure. The crude was dissolved in EtOH (10 mL), cooled to 0 °C and cold water (1 – 2 mL) was added to the mixture resulting in the appearance of a precipitate. The solid was filtered off, washed with cold water and dried to provide ethyl 2-(phenylamino)acetate **1**[32] (1.16 g, 54 %) as a dark solid. ^{1}H NMR (400 MHz, $CDCl_3$) δ 1.30 (t, J = 7.1 Hz, 3H, H_8), 3.91 (s, 2H, H_2), 4.25 (q, J = 7.1 Hz, 2H, H_7), 6.60 – 6.67 (m, 2H, H_5), 6.77 (td, J = 1.1, 7.3 Hz, 1H, H_6), 7.15 – 7.24 (m, 2H, H_4). To a solution of amine **1** (872.3 mg, 4.87 mmol) in dry THF (10 mL) at 0 °C, was added Et_3N (2.04 mL, 14.60 mmol) and acryloyl chloride (475 µL, 5.84 mmol). The reaction was stirred at 0 °C for 3 h and the solid was filtered off. The filtrate was concentrated under reduced pressure and purified by flash chromatography on silica gel, eluting with cyclohexane/EtOAc (7/3, v/v) to provide ethyl 2-(*N*-phenylprop-2-enamido)acetate **2** (876 mg, 77 %) as a yellow oil. ^{1}H NMR (400 MHz, $CDCl_3$) δ 1.27 (t, J = 7.1 Hz, 3H, H_8), 4.20 (q, J = 7.2 Hz, 2H, H_7), 4.45 (s, 2H, H_2), 5.57 (dd, J = 2.0, 10.3 Hz, $H_{11trans}$), 6.09 (dd, J = 10.3, 16.8 Hz, 1H, H_{10}), 6.41 (dd, J = 1.9, 16.8 Hz, 1H, H_{11cis}), 7.30 – 7.45 (m, 5H, H_{4-6}). ^{13}C NMR (101 MHz, $CDCl_3$) δ 14.3 (C_8), 51.7 (C_2),

61.4 (C$_7$), 127.9 (C$_{10}$), 128.2 (C$_{ar}$), 128.6 (C$_{11}$), 129.8 (C$_{ar}$), 142.3 (C$_3$), 166.0 (C$_9$), 169.1 (C$_1$).

To a solution of acrylamide **2** (876 mg, 3.76 mmol) in EtOH (10 mL), was added *tert*-butylamine (1.58 mL, 15.02 mmol). The reaction was stirred at 55 °C for 16 h, then concentrated under reduced pressure. The crude ethyl 2-[3-(*tert*-butylamino)-*N*-phenylpropanamido]acetate **3** (1.067 g, 93 %) obtained as a yellow oil was used in the next step without further purification. ^{1}H NMR (400 MHz, CDCl$_3$) δ 1.07 (s, 9H, H$_{13}$), 1.26 (t, *J* = 7.2 Hz, 3H, H$_8$), 2.33 (t, *J* = 6.7 Hz, 2H, H$_{10}$), 2.78 (t, *J* = 6.7 Hz, 2H, H$_{11}$), 4.19 (q, *J* = 7.2 Hz, 2H, H$_7$), 4.34 (s, 2H, H$_2$), 7.31 – 7.43 (m, 5H, H$_{4-6}$). ^{13}C NMR (101 MHz, CDCl$_3$) δ 14.3 (C$_8$), 29.0 (C$_{13}$), 35.4 (C$_{10}$), 38.4 (C$_{11}$), 50.6 (C$_{12}$), 51.4 (C$_2$), 61.4 (C$_7$), 128.3 (C$_4$), 128.5 (C$_6$), 129.9 (C$_5$), 142.7 (C$_3$), 169.3 (C$_1$), 172.8 (C$_9$). Compound **3** (644.5 mg, 2.10 mmol) was submitted to general procedure A. The crude was purified by flash chromatography, eluting with cyclohexane/EtOAc (4/6, v/v) to afford the expected compound **4** (546.0 mg, 75 %) as a pale yellow oil. ^{1}H NMR (400 MHz, CDCl$_3$) δ 1.21 – 1.32 (m, 12H, H$_8$ and H$_{13}$), 1.94 (s, 3H, H$_{15}$), 2.32 – 2.41 (m, 2H, H$_{10}$), 3.52 – 3.61 (m, 2H, H$_{11}$), 4.21 (q, *J* = 7.1 Hz, 2H, H$_7$), 4.34 (s, 2H, H$_2$), 7.31 – 7.48 (m, 5H, H$_{4-6}$). ^{13}C NMR (101 MHz, CDCl$_3$) δ 14.3 (C$_8$), 24.9 (C$_{15}$), 29.0 (C$_{13}$), 36.0 (C$_{10}$), 42.8 (C$_{11}$), 51.3 (C$_2$), 57.1 (C$_{12}$), 61.5 (C$_7$), 128.0 (C$_4$), 128.9 (C$_6$), 130.2 (C$_5$), 142.5 (C$_3$), 169.1 (C$_1$), 170.8 (C$_9$), 171.4 (C$_{14}$). HRMS (ESI): calc. for C$_{19}$H$_{29}$O$_4$N$_2$ [M+H]$^+$: 349.2122, found 349.2116.

Ethyl 2-(3-{*N*-*tert*-butyl-2-[3-(*N*-*tert*-butylacetamido)-*N*-phenylpropanamido]acetamido} -*N*-phenylpropanamido)acetate (6).

Compound **4** (220.0 mg, 0.63 mmol) was submitted to general procedure B to afford the crude 2-[3-(*N*-*tert*-butylacetamido)-*N*-phenylpropanamido]acetic acid **5** (97.0 mg, 48 %) as a white solid. ^{1}H NMR (400 MHz, CDCl$_3$) δ 1.28 (s, 9H, H$_{11}$), 1.97 (s, 3H, H$_{13}$), 2.33 – 2.44 (m, 2H, H$_8$), 3.55 – 3.61 (m, 2H, H$_9$), 4.38 (s, 2H, H$_2$), 7.31 – 7.50 (m, 5H, H$_{4-6}$). General procedure C was applied using carboxylic acid **5** (97.0 mg, 0.30 mmol) and amine **3** (91.9 mg,

The crude was purified by flash chromatography, eluting with cyclohexane/EtOAc (1/9, v/v) to provide the expected tetramer **6** (97.8 mg, 53 %) as a pale yellow gum. ^{1}H NMR (400 MHz, CDCl$_3$) δ 1.25 (d, J = 7.7 Hz, 21H, H$_{21}$ and H$_{10}$ and H$_{25}$), 1.90 (s, 3H, H$_{23}$), 2.30 – 2.38 (m, 2H, H$_{18}$), 2.41 – 2.48 (m, 2H, H$_7$), 3.44 – 3.56 (m, 4H, H$_8$ and H$_{19}$), 4.18 (q, J = 7.2 Hz, 2H, H$_{24}$), 4.22 (s, 2H, H$_{12}$), 4.31 (s, 2H, H$_2$), 7.28 – 7.48 (m, 10H, H$_{14-16}$ and H$_{4-6}$). ^{13}C NMR (101 MHz, CDCl$_3$) δ 14.3 (C$_{25}$), 24.9 (C$_{23}$), 28.8 (C$_{10}$), 28.9 (C$_{20}$), 35.9 (C$_7$), 36.1 (C$_{18}$), 41.0 (C$_8$), 43.0 (C$_{19}$), 51.4 (C$_2$), 53.1 (C$_{12}$), 57.0 (C$_9$), 57.7 (C$_{20}$), 61.5 (C$_{24}$), 128.0 (C$_4$), 128.2 (C$_{14}$), 128.4 (C$_6$), 128.8 (C$_{16}$), 129.8 (C$_5$), 130.1 (C$_{15}$), 142.4 (C$_3$), 143.2 (C$_{13}$), 167.5 (C$_{11}$), 169.0 (C$_1$), 170.3 (C$_{17}$), 170.7 (C$_6$), 171.5 (C$_{22}$). HRMS (ESI): calc. for C$_{34}$H$_{49}$O$_6$N$_4$ [M+H]$^+$: 609.3647, found 609.3650.

Ethyl 3-[2-(*N-tert*-butylacetamido)-*N*-phenylacetamido]propanoate (10).

To a solution of aniline (490 µL, 5.37 mmol) in water (1 mL), was added ethyl acrylate (16.11 mmol, 1.78 mL), and trifluoroethanol (10.74 mmol, 782 µL). After one night at reflux, the reaction was cooled to room temperature and extracted with EtOAc. The organic layer was dried over Na$_2$SO$_4$ and concentrated under reduced pressure. The crude was purified by flash chromatography, eluting with cyclohexane/EtOAc (8/2, v/v) to yield ethyl 3-(phenylamino)propanoate **7**[33] (635.5 mg, 61 %) as a pale yellow oil. ^{1}H NMR (400 MHz, CDCl$_3$) δ 1.26 (t, J = 7.2 Hz, 3H, H$_9$), 2.61 (t, J = 6.4 Hz, 2H, H$_2$), 3.46 (t, J = 6.4 Hz, 2H, H$_3$), 4.09 (s, 1H, NH), 4.16 (q, J = 7.1 Hz, 2H, H$_8$), 6.61 – 6.66 (m, 2H, H$_5$), 6.72 (tt, J = 1.1, 7.3 Hz, 1H, H$_7$), 7.15 – 7.22 (m, 2H, H$_6$). To a solution of **7** (661 mg, 3.42 mmol) in dry THF (5 mL) at – 20 °C, was added Et$_3$N (4.11 mmol, 573 µL) and bromoacetyl bromide (4.11 mmol, 358 µL). The reaction was stirred at – 20 °C for 2 – 3 h. After completion, monitored by TLC, the reaction was filtered and the filtrate was concentrated under reduced pressure. The crude was purified by flash chromatography, eluting with cyclohexane/EtOAc (6/4, v/v) to provide ethyl 3-(2-bromo-*N*-phenylacetamido)propanoate **8** (633.0 mg, 59 %) as

a pale yellow oil. ^{1}H NMR (400 MHz, CDCl$_3$) δ 1.20 (t, J = 7.1 Hz, 3H, H$_9$), 2.60 (t, J = 7.3 Hz, 2H, H$_2$), 3.62 (s, 2H, H$_{11}$), 3.97 – 4.10 (m, 4H, H$_3$ and H$_8$), 7.26 – 7.30 (m, 2H, H$_6$), 7.36 – 7.51 (m, 3H, H$_5$ and H$_7$). ^{13}C NMR (101 MHz, CDCl$_3$) δ 14.2 (C$_6$), 27.2 (C$_{11}$), 32.7 (C$_2$), 46.2 (C$_3$), 60.8 (C$_8$), 128.2 (C$_6$), 129.0 (C$_7$), 130.2 (C$_5$), 141.3 (C$_4$), 166.6 (C$_{10}$), 171.3 (C$_1$). To a solution of **8** (633 mg, 2.01 mmol) in dry THF (5 mL) at room temperature, was added Et$_3$N (4.03 mmol, 562 µL) and *tert*-butylamine (8.06 mmol, 847 µL). The reaction was stirred overnight. After completion, monitored by TLC, the reaction was filtered and the liquid was concentrated under reduced pressure. The crude ethyl 3-[2-(*tert*-butylamino)-*N*-phenylacetamido]propanoate **9** (582 mg, 94 %) obtained as a pale yellow oil was engaged in the next step without purification. ^{1}H NMR (400 MHz, CDCl$_3$) δ 0.99 (s, 9H, H$_{12}$), 1.19 (t, J = 7.1 Hz, 3H, H$_9$), 2.58 (t, J = 7.4 Hz, 2H, H$_2$), 3.05 (s, 2H, H$_{11}$), 4.03 (m, 4H, H$_3$ and H$_8$), 7.14 – 7.21 (m, 2H, H$_6$), 7.34 – 7.51 (m, 3H, H$_5$ and H$_7$). ^{13}C NMR (101 MHz, CDCl$_3$) δ 14.2 (C$_9$), 28.5 (C$_{12}$), 32.9 (C$_2$), 44.7 (C$_{11}$), 45.7 (C$_2$), 50.9 (C$_{13}$), 60.7 (C$_8$), 128.2 (C$_6$), 128.7 (C$_7$), 130.1 (C$_5$), 140.9 (C$_4$), 171.1 (C$_{10}$), 171.4 (C$_1$). Compound **9** (639 mg, 2.09 mmol) was submitted to general procedure A. The crude was purified by flash chromatography on silica gel, eluting with EtOAc/cyclohexane (6/4, v/v) to afford compound **10** (565.3 mg, 78 %) as a yellow oil. ^{1}H NMR (400 MHz, CDCl$_3$) δ 1.20 (t, J = 7.1 Hz, 3H, H$_9$), 1.36 (s, 9H, H$_{12}$), 1.97 (s, 3H, H$_{13}$), 2.57 (t, J = 7.1 Hz, 2H, H$_2$), 3.69 (s, 2H, H$_{11}$), 3.93 – 4.12 (m, 4H, H$_8$ and H$_3$), 7.21 – 7.25 (m, 2H, H$_6$), 7.37 – 7.53 (m, 3H, H$_5$ and H$_7$). ^{13}C NMR (101 MHz, CDCl$_3$) δ 14.2 (C$_9$), 25.1 (C$_{13}$), 28.6 (C$_{12}$), 33.1 (C$_2$), 45.9 (C$_3$), 49.2 (C$_{11}$), 57.3 (C$_{14}$), 60.8 (C$_8$), 128.2 (C$_6$), 129.1 (C$_7$), 130.5 (C$_5$), 140.9 (C$_4$), 169.1 (C$_{10}$), 171.4 (C$_1$ or C$_{15}$), 171.8 (C$_1$ or C$_{15}$). HRMS (ESI): calc. for C$_{19}$H$_{29}$O$_4$N$_2$ [M+H]$^+$: 349.2122, found 349.2115.

Ethyl 3-(2-{*N*-*tert*-butyl-3-[2-(*N*-*tert*-butylacetamido)-*N*-phenylacetamido]propanamido}-*N*-phenylacetamido)propanoate (12).

^{1}H NMR (400 MHz, CDCl$_3$) δ 1.35 (s, 9H, H$_{11}$), 1.99 (s, 3H, H$_{13}$), 2.58 (t, J = 6.8 Hz, 2H, H$_2$), 3.71 (s, 2H, H$_9$), 4.03 (s, 2H, H$_3$), 7.27 (s, 2H, H$_6$), 7.47 (m, 3H, H$_5$ and H$_7$). The general procedure C was applied using the carboxylic acid **11** (50 mg, 0.16 mmol) and the amine **9** (50 mg, 0.16 mmol). The crude was purified by flash chromatography on silica gel, eluting with EtOAc to afford the tetramer **12** (43.2 mg, 46 %) as a yellow gum. ^{1}H NMR (400 MHz, CDCl$_3$) δ 1.20 (t, J = 7.1 Hz, 3H, H$_{14}$), 1.31 (s, 9H, H$_{20}$), 1.38 (s, 9H, H$_{26}$), 2.01 (s, 3H, H$_{12}$), 2.50 – 2.60 (m, 4H, H$_2$ and H$_7$), 3.73 (s, 2H, H$_{10}$), 3.88 (s, 4H, H$_5$ and H$_8$), 4.00 (t, J = 7.3 Hz, 2H, H$_3$), 4.06 (q, J = 7.1 Hz, 2H, H$_{13}$), 7.23 (d, J = 7.6 Hz, 2H, H$_{22}$), 7.33 (d, J = 7.5 Hz, 2H, H$_{16}$), 7.38 – 7.52 (m, 6H, H$_{ar}$). ^{13}C NMR (101 MHz, CDCl$_3$) δ 14.3 (C$_{14}$), 25.2 (C$_{12}$), 28.5 (C$_{20}$), 28.7 (C$_{26}$), 33.0 (C$_2$), 35.1 (C$_7$), 45.9 (C$_3$), 47.5 (C$_5$ or C$_8$), 48.5 (C$_5$ or C$_8$), 49.2 (C$_{10}$), 57.3 (C$_{25}$), 57.7 (C$_{19}$), 60.8 (C$_{13}$), 128.0 (C$_{22}$), 128.4 (C$_{15}$), 128.8 (C$_{24}$), 129.1 (C$_{18}$), 130.3 (C$_{23}$), 130.5 (C$_{17}$), 140.7 (C$_{15}$), 141.5 (C$_{21}$), 169.2 (C$_9$ or C$_5$ or C$_4$), 169.3 (C$_9$ or C$_5$ or C$_4$), 171.3 (C$_1$), 171.5 (C$_9$ or C$_5$ or C$_4$), 171.9 (C$_{11}$).

Ethyl 2-(*N-tert*-butylprop-2-enamido)acetate (14).

To a solution of ethylbromo acetate (1.33 mL, 11.98 mmol) in dry THF (20 mL) at room temperature, was added Et$_3$N (3.34 mL, 23.95 mmol) and *tert*-butylamine (5.03 mL, 47.90 mmol). The reaction was stirred overnight. After completion, monitored by TLC, the reaction was filtered and the liquid was concentrated under reduced pressure. The crude ethyl 2-(*tert*-butylamino)acetate **13** (1.17 g, 62 %, colorless oil) was used in the next step without further purification. ^{1}H NMR (400 MHz, CDCl$_3$) δ 1.04 (s, 9H, H$_4$), 1.21 (t, J = 7.1 Hz, 3H, H$_6$), 3.33 (s, 2H, H$_2$), 4.12 (q, J = 7.2 Hz, 2H, H$_5$). To a solution of amine **13** (500.0 mg, 3.14 mmol) in dry THF (20 mL) at 0 °C, was added Et$_3$N (1.31 mL, 9.42 mmol) and acryloyl chloride

(306 µL, 3.78 mmol). The reaction was stirred at 0° C for 2 h and the solid was filtered off. The filtrate was concentrated under reduced pressure and purified by flash chromatography on silica gel, eluting with cyclohexane/EtOAc (7/3, v/v) to provide the expected compound **14** (524.4 mg, 78.3 %) as a yellow oil. ^{1}H NMR (400 MHz, CDCl$_3$) δ 1.29 (t, J = 7.1 Hz, 3H, H$_9$), 1.45 (s, 9H, H$_4$), 4.11 (s, 3H, H$_2$), 4.22 (q, J = 7.1 Hz, 2H, H$_8$), 5.58 (dd, J = 1.9, 10.5 Hz, 1H, H$_{7trans}$), 6.18 (dd, J = 2.0, 16.8 Hz, 1H, H$_6$), 6.38 (dd, J = 10.4, 16.8 Hz, 1H, H$_{7cis}$)

Ethyl 2-[*N*-*tert*-butyl-3-(*N*-phenylacetamido)propanamido]acetate (17).

Compound **7** (434 mg, 2.24 mmol) was submitted to general procedure A. The crude was purified by flash chromatography, eluting with EtOAc/cyclohexane (3/7, v/v) to provide ethyl 3-(*N*-phenylacetamido)propanoate **15** (482 mg, 91 %) as a colorless oil. ^{1}H NMR (400 MHz, CDCl$_3$) δ 1.19 (t, J = 7.1 Hz, 3H, H$_{11}$), 1.82 (s, 3H, H$_9$), 2.57 (t, J = 7.3 Hz, 2H, H$_2$), 3.97 – 4.08 (m, 4H, H$_3$ and H$_{10}$), 7.17 (d, J = 7.5 Hz, 2H, H$_6$), 7.34 (m, 1H, H$_7$), 7.42 (t, J = 7.5 Hz, 2H, H$_5$). ^{13}C NMR (101 MHz, CDCl3) δ 14.2 (C$_{11}$), 22.8 (C$_9$), 33.1 (C$_2$), 45.2 (C$_3$), 60.7 (C$_{10}$), 128.3 (C$_{ar}$), 129.9 (C$_{ar}$), 142.9 (C$_{ar}$), 170.5 (C$_8$), 171.6 (C$_1$). Compound **15** (482.0 mg, 2.05 mmol) was submitted to general procedure B to afford the crude 3-(*N*-phenylacetamido)propanoic acid **16** (340.0 mg, 80 %) as a white solid. ^{1}H NMR (400 MHz, CDCl$_3$) δ 1.84 (s, 3H, H$_9$), 2.62 (t, J = 7.2 Hz, 2H, H$_2$), 4.00 (t, J = 7.2 Hz, 2H, H$_3$), 7.19 (dd, J = 1.7, 7.3 Hz, 2H, H$_{ar}$), 7.32 – 7.47 (m, 3H, H$_{ar}$). ^{13}C NMR (101 MHz, CDCl$_3$) δ 22.7 (C$_9$), 32.8 (C$_2$), 45.4 (C$_3$), 128.1 (C$_{ar}$), 128.5 (C$_{ar}$), 130.1 (C$_{ar}$), 142.5 (C$_4$), 171.5 (C$_8$), 175.6 (C$_2$). General procedure C was applied using carboxylic acid **16** (100.0 mg, 0.48 mmol) and monomer amine **13** (76.4 mg, 0.48 mmol). The crude was purified by flash chromatography, eluting with cyclohexane/EtOAc (3/7, v/v) to provide dimer **17** (146 mg, 87 %) as a white solid. ^{1}H NMR (400 MHz, CDCl$_3$) δ 1.27 (t, J = 7.2 Hz, 3H, H$_{15}$), 1.37 (s, 9H, H$_4$), 1.82 (s, 3H, H$_{13}$), 2.56 (bs, 2H, H$_6$), 3.95 (t, J = 7.6 Hz, 2H, H$_7$), 4.10 (s, 2H, H$_2$), 4.20 (q, J = 7.2 Hz, 2H, H$_{14}$), 7.09 – 7.18 (m, 2H, H$_9$), 7.29 – 7.43 (m, 3H, H$_{10}$ and H$_{11}$). ^{13}C NMR (101 MHz,

CDCl$_3$) δ 14.3 (C$_{15}$), 22.9 (C$_{13}$), 28.7 (C$_4$), 34.2 (C$_6$), 46.6 (C$_7$), 47.4 (C$_2$), 57.8 (C$_3$), 61.6 (C$_{14}$),128.0 (C$_{10}$ and C$_{11}$), 129.8 (C$_9$), 143.4 (C$_8$), 170.7 (C$_{12}$), 170.8 (C$_1$), 171.7 (C$_5$).

Ethyl 2-(*N-tert*-butyl-3-{2-[*N-tert*-butyl-3-(*N*-phenylacetamido)propanamido]-*N*-phenylacetamido}propanamido)acetate (19).

Compound **17** (146.0 mg, 0.42 mmol) was submitted to general procedure B to afford the crude 2-[*N-tert*-butyl-3-(*N*-phenylacetamido)propanamido]acetic acid (103.0 mg, 77 %) as a withe solid. ^{1}H NMR (400 MHz, CDCl$_3$) δ 1.41 (s, 9H, H$_4$), 1.87 (s, 3H, H$_{13}$), 2.66 (t, J = 7.9 Hz, 2H, H$_6$), 3.96 (t, J = 7.6 Hz, 2H, H$_7$), 4.16 (s, 2H, H$_2$), 7.20 (d, J = 7.6 Hz, 2H, H$_{ar}$), 7.39 (m, 3H, H$_{ar}$). The general procedure D was applied using the crude 2-[*N-tert*-butyl-3-(*N*-phenylacetamido)propanamido]acetic acid (100.0 mg, 0.31 mmol,) and the monomer amine **7** (59.9 mg, 0.31 mmol). The crude was purified by flash chromatography, eluting with cyclohexane/EtOAc (3/7, v/v) to provide ethyl 3-{2-[*N-tert*-butyl-3-(*N*-phenylacetamido)propanamido]-*N*-phenylacetamido} propanoate **18** (80 mg, 52 %) as a colorless oil. ^{1}H NMR (400 MHz, CDCl$_3$) δ 1.18 – 1.23 (m, 3H, H$_{22}$), 1.31 (s, 9H, H$_{11}$), 1.84 (s, 3H, H$_{20}$), 2.52 (m, 2H, H$_{13}$), 2.59 (t, J = 7.4 Hz, 2H, H$_2$), 3.79 (s, 2H, H$_9$), 3.91 (m, 2H, H$_{14}$), 3.97 – 4.12 (m, 4H, H$_3$ and H$_{21}$), 7.19 (d, J = 7.7 Hz, 2H, H$_{ar}$), 7.28 – 7.57 (m, 8H, H$_{ar}$). ^{13}C NMR (101 MHz, CDCl3) δ 14.3 (C$_{23}$), 23.0 (C$_{20}$), 28.6 (C$_{11}$), 33.0 (C$_2$), 34.5 (C$_{13}$), 45.9 (C$_3$), 48.3 (C$_{14}$), 57.5 (C$_{15}$), 60.8 (C$_{21}$), 128.0 (C$_{ar}$), 128.1 (C$_{ar}$), 128.3 (C$_{ar}$), 129.0 (C$_{ar}$), 129.8 (C$_{ar}$), 130.4 (C$_{ar}$), 140.9 (C$_{ar}$), 143.6 (C$_{ar}$), 169.2 (C$_8$), 170.7 (C$_{19}$), 171.4 (C$_1$), 171.8 (C$_{12}$).

The general procedure B was applied using the ester **18** (60 mg 0.12 mmol) to afford the crude ethyl 3-{2-[*N-tert*-butyl-3-(*N*-phenylacetamido)propanamido]-*N*-phenylacetamido}propanoic acid (44.0 mg, 77 %) as a white solid.^{1}H NMR (400 MHz, CDCl$_3$) δ 1.28 (s, 9H, H$_{11}$), 1.94 (s, 3H, H$_{20}$), 2.47 (m, 4H, H$_2$ and H$_{13}$), 3.68 (s, 2H, H$_9$), 4.03 (bs, 4H, H$_3$ and H$_{14}$), 7.28 – 7.66 (m, 10H, H$_{ar}$). The general procedure D was applied using ethyl 3-{2-[*N-tert*-butyl-3-(*N*-phenylacetamido)propanamido]-*N*-phenylacetamido}propanoic

The crude was purified by flash chromatography, eluting with cyclohexane/EtOAc (3/7, v/v) to afford the expected tetramer **19** (80 mg, 52 %) as a colorless oil. ^{1}H NMR (400 MHz, CDCl$_3$) δ 1.26 (t, J = 7.1 Hz, 3H, H$_{26}$), 1.31 (s, 9H, H$_{15}$), 1.38 (s, 9H, H$_4$), 1.83 (s, 3H, H$_{24}$), 2.52 (bs, 2H, H$_{17}$), 2.60 (bs, 2H, H$_6$), 3.79 (s, 2H, H$_{13}$), 3.91 (t, J = 7.0 Hz, 2H, H$_{18}$), 3.99 (t, J = 7.0 Hz, 2H, H$_7$), 4.13 (s, 2H, H$_2$), 4.19 (q, J = 7.1 Hz, 2H, H$_{25}$), 7.15 – 7.22 (m, 2H, H$_{ar}$), 7.27 – 7.50 (m, 7H, H$_{ar}$). ^{13}C NMR (101 MHz, CDCl3) δ 14.3 (C$_{26}$), 23.0 (C$_{24}$), 28.6 (C$_{15}$), 28.7 (C$_4$), 34.2 (C$_6$), 34.6 (C$_{17}$), 46.9 (C$_{18}$), 47.0 (C$_7$), 47.4 (C$_2$), 48.4 (C$_{13}$), 57.6 (C$_{14}$), 57.8 (C$_3$), 61.6 (C$_{25}$), 127.9 (C$_{Ar}$), 128.1 (C$_{Ar}$), 128.2 (C$_{Ar}$), 128.8 (C$_{Ar}$), 129.8 (C$_{Ar}$), 130.3 (C$_{Ar}$), 141.5 (C$_{Ar}$), 143.6 (C$_{Ar}$), 169.2 (C$_{12}$), 170.6 (C$_{24}$), 170.9 (C$_1$), 171.5 (C$_5$ or C$_{16}$), 171.6 (C$_5$ or C$_{16}$).

Ethyl 3-[*N-tert*-butyl-2-(phenylamino)acetamido]propanoate (22).

To a solution of ethylacrylate (10.00 g, 99.88 mmol) in EtOH (0.2 M) at room temperature, was added *t*BuNH$_2$ (29.22 g, 42 mL, 4 equiv.). After stirring for 16 h at 60 °C, the mixture was cooled down then concentrated and dried *in vacuo*, yielding the crude ethyl 3-(*tert*-butylamino)propanoate **20**. The crude was purified on flash chromatography, eluting with cyclohexane/EtOAc (8/2, v/v) to provide the expected compound **20** (14.47 g, 83.51 mmol, 84 %) as a colorless oil. ^{1}H NMR (400 MHz, CDCl$_3$) δ 1.11 (s, 9H, H$_9$), 1.26 (t, *J* = 6.8 Hz, 3H, H$_7$), 2.49 (t, *J* = 6.5 Hz, 2H, H$_2$), 2.82 (t, *J* = 6.6 Hz, 2H, H$_3$), 4.14 (q, *J* = 7.2 Hz, 2H, H$_6$). ^{13}C NMR (101 MHz, CDCl$_3$) δ 14.4 (C$_7$), 29.1 (C$_5$), 35.8 (C$_2$), 38.2 (C$_3$), 50.6 (C$_4$), 60.5 (C$_6$), 173.1 (C$_1$). To a solution of **20** (1.02 g, 5.88 mmol,) in dry THF (5 mL) at - 20 °C, was added Et$_3$N (985 μL, 7.07 mmol) and bromoacetyl bromide (615 μL, 7.07 mmol). The reaction was stirred at - 20 °C for 2 – 3 h. After completion, monitored by TLC, the reaction was filtered and the liquid was concentrated under reduced pressure. The crude was purified on flash chromatography, eluting with cyclohexane/EtOAc (8/2, v/v) to provide ethyl 3-(2-bromo-*N-*

tert-butylacetamido)propanoate **21** (1.33 g, 77 %) as a pale yellow oil. ^{1}H NMR (400 MHz, CDCl$_3$) δ 1.27 (t, J = 7.3 Hz, 3H, H$_7$), 1.45 (s, 9H, H$_5$), 2.60 – 2.67 (m, 2H, H$_2$), 3.64 – 3.76 (m, 2H, H$_3$), 3.91 (s, 2H, H$_9$), 4.16 (q, J = 7.2 Hz, 2H, H$_6$). ^{13}C NMR (101 MHz, CDCl$_3$) δ 14.3 (C$_7$), 28.7 (C$_5$), 29.9 (C$_9$), 36.9 (C$_2$), 41.9 (C$_3$), 58.1 (C$_4$), 61.2 (C$_6$), 167.5 (C$_8$), 170.8 (C$_1$). To a solution of **21** (665.0 mg, 2.26 mmol) in dry THF (5 mL) was added Et$_3$N (4.52 mmol, 631 µL) and aniline (9.04 mmol, 826 µL). The reaction was stirred at room temperature for 3 days. After completion, monitored by TLC, the reaction was filtered and the liquid was concentrated under reduced pressure. The crude was purified on flash chromatography, eluting with cyclohexane/EtOAc (7/3, v/v) to provide the expected compound **22** (541 mg, 78 %) as a colorless oil. ^{1}H NMR (400 MHz, CDCl$_3$) δ 1.29 (t, J = 7.1 Hz, 3H, H$_{13}$), 1.49 (s, 9H, H$_5$), 2.61 (dd, J = 6.8, 9.3 Hz, 2H, H$_2$), 3.65 (dd, J = 6.7, 9.5 Hz, 2H, H$_3$), 3.90 (s, 2H, H$_7$), 4.18 (q, J = 7.2 Hz, 2H, H$_{12}$), 6.67 (d, J = 7.9 Hz, 2H, H$_{10}$), 6.74 (t, J = 7.4 Hz, 1H, H$_{11}$), 7.20 (t, J = 7.4 Hz, 2H, H$_9$). ^{13}C NMR (101 MHz, CDCl3) δ 14.3 (C$_{13}$), 28.9 (C$_5$), 36.5 (C$_2$), 39.8 (C$_3$), 47.5 (C$_7$), 58.1 (C$_4$), 61.2 (C$_{12}$), 113.6 (C$_{10}$), 118.1 (C$_{11}$), 129.4 (C$_9$), 147.2 (C$_8$), 169.2 (C$_6$), 170.8 (C$_1$). <mark>HRMS (ESI): calc. for C$_{17}$H$_{27}$N$_2$O$_3$ [M+H]$^+$: 307.2016, found 307.2019.</mark>

Ethyl 3-(*N*-*tert*-butyl-2-{3-[*N*-*tert*-butyl-2-(*N*-phenylacetamido)acetamido]-*N*-phenylpropanamido}acetamido)propanoate (27).

To a solution of **22** (541.0 mg, 1.77 mmol,) in dry THF (5 mL) at 0 °C, was added Et$_3$N (738 µL, 5.30 mmol) and acryloyl chloride (172 µL, 2.12 mmol). The reaction was stirred at 0 °C for 3 h. After completion, monitored by TLC, the reaction was filtered and the liquid was concentrated under reduced pressure. The crude was purified by flash chromatography, eluting with cyclohexane/EtOAc (1/1, v/v) to provide ethyl 3-[*N*-*tert*-butyl-2-(*N*-phenylprop-2-enamido)acetamido]propanoate **23** (617 mg, 97 %) as a pale yellows oil. ^{1}H NMR (400 MHz, CDCl$_3$) δ 1.25 (t, J = 7.1 Hz, 3H, H$_{16}$), 1.44 (s, 9H, H$_5$), 2.67 – 2.76 (m, 2H, H$_2$), 3.56 –

3.67 (m, 2H, H_3), 4.12 (q, J = 7.2 Hz, 2H, H_{15}), 4.50 (s, 2H, H_{15}), 5.54 (d, J = 10.4 Hz, 1H, H_{14}), 6.13 (dd, J = 10.6, 16.2 Hz, 1H, H_{13}), 6.37 (d, J = 16.8 Hz, 1H, H_{14}), 7.29 – 7.44 (m, 5H, H_{ar}). ^{13}C NMR (101 MHz, CDCl3) δ 14.3 (C_{16}), 29.0 (C_5), 36.3 (C_2), 40.3 (C_3), 53.7 (C_7), 57.9 (C_4), 61.0 (C_{15}), 127.8 (C_{14}), 128.0 (C_{13}), 128.3 (C_{ar}), 128.4 (C_{ar}), 129.5 (C_{ar}), 143.1 (C_8), 166.0 (C_{12}), 167.8 (C_6), 171.1 (C_1). To a solution of **23** (617.0 mg, 1.71 mmol) in EtOH (10 mL) at room temperature, was added tBuNH$_2$ (720 µL, 6.85 mmol). The reaction was stirred at 65°C for 16 h. After completion, monitored by TLC, the reaction was concentrated under reduced pressure. The crude ethyl 3-{*N*-*tert*-butyl-2-[3-(*tert*-butylamino)-*N*-phenylpropanamido]acetamido}propanoate **24** (659 mg, 89 %) obtained as a pale yellows oil was used in the next step without further purification. ^1H NMR (400 MHz, CDCl$_3$) δ 1.09 (s, 9H, H_{16}), 1.24 (t, J = 7.2 Hz, 3H, H_{18}), 1.43 (s, 9H, H_5), 2.38 (t, J = 6.9 Hz, 2H, H_{13}), 2.65 (dd, J = 6.6, 9.7 Hz, 2H, H_2), 2.81 (t, J = 6.7 Hz, 2H, H_{14}), 3.58 (dd, J = 6.6, 9.7 Hz, 2H, H_3), 4.11 (q, J = 7.3 Hz, 2H, H_{17}), 4.40 (s, 2H, H_7), 7.27 – 7.50 (m, 5H, H_{ar}). ^{13}C NMR (101 MHz, CDCl3) δ 14.3 (C_{18}), 28.8 (C_{15}), 29.0 (C_5), 35.1 (C_{13}), 36.3 (C_2), 38.6 (C_{14}), 40.2 (C_3), 53.4 (14), 51.0 (C_{15}), 57.9 (C_4), 61.0 (C_{17}), 128.1 (C_{ar}), 128.4 (C_{ar}), 129.7 (C_{ar}), 143.3 (C_8), 167.9 (C_6), 171.1 (C_1), 172.5 (C_{12}). To a solution of **24** (659 mg, 1.52 mmol) in dry THF (5 mL) at – 20 °C, was added Et$_3$N (254 µL, 1.82 mmol) and bromoacetyl bromide (159 µL, 1.82 mmol). The reaction was stirred at – 20 °C for 2 – 3 h. After completion, monitored by TLC, the reaction was filtered and the liquid was concentrated under reduced pressure. The crude was purified by flash chromatography, eluting with cyclohexane/EtOAc (1/1, v/v) to provide ethyl 3-{2-[3-(2-bromo-*N*-*tert*-butylacetamido)-*N*-phenylpropanamido]-*N*-tert-butylacetamido}propanoate **25** (283 mg, 34 %) as a pale yellow oil. ^1H NMR (400 MHz, CDCl$_3$) δ 1.25 (t, J = 7.1 Hz, 3H, H_{20}), 1.30 (s, 9H, H_{16} or H_5), 1.44 (s, 9H, H_{16} or H_5), 2.37 – 2.50 (m, 2H, H_{13}), 2.56 – 2.72 (m, 2H, H_2), 3.54 – 3.65 (m, 4H, H_3 and H_{14}), 3.67 (s, 2H, H_{18}), 4.12 (q, J = 7.2 Hz, 2H, H_{19}), 4.41 (s, 2H, H_7), 7.34 – 7.46 (m, H_{ar}). ^{13}C NMR (101 MHz,

CDCl3) δ 14.31 (C_{19}), 28.59 (C_{16} or C_5), 28.99 (C_{16} or C_5), 30.20 (C_{16}), 36.33 (C_2), 36.75 (C_{13}), 40.27 (C_3), 42.65 (C_{14}), 53.44 (C_7), 57.97 (C_{15} or C_4), 58.03 (C_{15} or C_4), 61.03 (C_{19}), 128.27 (C_{ar}), 128.69 (C_{ar}), 130.06 (C_{ar}), 143.17 (C_8), 167.43 (C_6), 167.46 (C_{17}), 170.31 (C_{12}), 171.06 (C_1). To a solution of **25** (283.0 mg, 0.51 mmol) in dry THF (5 mL) was added Et$_3$N (142 μL, 1.02 mmol) and aniline (186 μL, 2.04 mmol). The reaction was stirred at room temperature for 48 hours. After completion, monitored by TLC, the reaction was filtered and the liquid was concentrated under reduced pressure. The crude was purified by flash chromatography, eluating with cyclohexane/EtOAc (6/4, v/v) to provide ethyl 3-(*N*-*tert*-butyl-2-{3-[*N*-*tert*-butyl-2-(phenylamino)acetamido]-*N*-phenylpropanamido}acetamido)propanoate **26** (183 mg, 63 %) as a pale yellow oil. ^{1}H NMR (400 MHz, CDCl$_3$) δ 1.26 (t, J = 7.1 Hz, 3H, H_{24}), 1.33 (s, 9H, H_5), 1.45 (s, 9H, H_{16}), 2.39 – 2.48 (m, 2H, H_{13}), 2.59 – 2.71 (m, 2H, H_2), 3.59 (t, J = 7.0 Hz, 4H, H_3 and H_{14}), 3.78 (s, 2H, H_{18}), 4.13 (q, J = 7.1 Hz, 2H, H_{23}), 4.42 (s, 2H, H_7), 6.65 – 6.84 (m, 3H, H_{ar}), 7.17 – 7.24 (m, 2H, H_{ar}), 7.28 – 7.49 (m, 5H, H_{ar}). ^{13}C NMR (101 MHz, CDCl$_3$) δ 14.3 (C_{24}), 28.8 (C_5), 29.0 (C_{16}), 36.0 (C_{13}), 36.4 (C_2) 40.3 (C_3), 40.7 (C_{14}), 47.7 (C_{18}), 53.5 (C_7), 58.0 (C_{16}), 58.1 (C_5), 61.4 (C_{23}), 114.2 (C_{Ar}), 128.1 (C_{Ar}), 128.7 (C_{Ar}), 129.4 (C_{Ar}), 130.1 (C_{Ar}), 143.1 (C_{Ar}), 167.5 (C_6), 168.9 (C_{17}), 170.4 (C_{12}), 171.0 (C_1). The general procedure A was applied using compound **26** (183.0 mg, 0.32 mmol) as starting material. The crude was purified by flash chromatography, eluting with cyclohexane/EtOAc (3/7, v/v) to afford the expected compound **27** (167 mg, 85 %) as a pink oil. ^{1}H NMR (400 MHz, CDCl$_3$) δ 1.20 – 1.29 (m, 12H, H_{26} and H_{16}), 1.43 (s, 9H, H_5), 1.89 (s, 3H, H_{24}), 2.44 – 2.52 (m, 2H, H_{13}), 2.60 – 2.69 (m, 2H, H_2), 3.48 – 3.54 (m, 2H, H_{14}), 3.54 – 3.60 (m, 2H, H_3), 4.12 (q, J = 7.1 Hz, 2H, H_{25}), 4.20 (s, 2H, H_{18}), 4.38 (s, 2H, H_7), 7.27 – 7.45 (m, H_{ar}). ^{13}C NMR (101 MHz, CDCl3) δ 14.3 (C_{26}), 22.4 (C_{24}), 28.8 (C_{16}), 29.0 (C_5), 36.1 (C_{13}), 36.3 (C_2), 40.3 (C_3), 41.2 (C_{14}), 53.1 (C_{18}), 53.4 (C_7), 57.7 (C_{15}), 57.9 (C_4), 61.0 (C_{25}), 127.8 (C_{ar}), 128.2 (C_{ar}), 128.3 (C_{ar}), 128.4 (C_{ar}), 129.5 (C_{ar}), 129.9 (C_{ar}), 143.2 (C_8),

144.3 (C_{19}), 167.6 (C_6), 168.0 (C_{17}), 170.6 (C_{12} and C_{23}), 171.0 (C_1). HRMS (ESI): calc. for $C_{34}H_{49}O_6N_4$ [M+H]$^+$: 609.3647, found 609.3742.

Computational Details.

Preparation of structures for quantum calculations. The structures for quantum calculations were prepared with the help of gauss view package.[34] The ω dihedral angle was considered to be in *cis* conformation for *Nt*Bu residues and *trans* for *N*Ph residues. Dihedrals angles were initially set from those determined by X–ray crystallography of oligopeptoids that display an analogy of backbone. All oligomers were capped with acyl and NMe$_2$ group at N- and C-termini, respectively, in order to mimic a full polypeptide backbone and avoid spurious capping effects. This capping can from the ester termination of some oligopeptoids synthetized.

Quantum calculation. All quantum calculations were performed with Gaussian09 suite of programs.[35] All full optimizations, as well as frequency calculations, were performed at Density Functional Theory (DFT) level M06-2X hybrid meta-GGA functional.[36] Carbon and hydrogen atoms were represented with the polarized all electron 6-311G(d,p) basis sets while nitrogen and oxygen atoms were represented with the augmented and polarized all electron 6-311++G(d,p) basis sets.[37] No symmetry nor geometry constrain was included during the optimization. Implicit solvent environment was considered using the SMD solvent model parameterized for dichloromethane.[38] The energetics related to a φ dihedral angle sign change has been assessed by means of a relaxed energy scan was performed for this angle. The scan was performed from 90º to –90º with increment of 5º at restricted Hartee Fock level using Ahlrichs-VDZ split valence basis set.[39] A single point energy calculation was then performed on the constrained optimized structure at DFT level using above mentioned functional and basis sets. All minima and transition states were finally fully optimized at M06-2X level using the polarized all electron 6-311G(d,p) basis set for all atoms.

Setup for Molecular Dynamics (MD) simulation. The Generalized AMBER Force Field (GAFF)[40] parameters were used to describe the potential of *Nt*Bu peptoid monomers. The RESP charges were generated using RED server[41] followed by the antechamber module[42] of AMBER to make the parameter/topology (parm) file. The peptoid oligomers were capped by acetyl group at N-terminus and N,N-dimethyl at C-terminus. The peptoid oligomers were solvated in acetonitrile box with a buffer of 16 Å towards each direction.

Molecular Dynamics simulation. All Molecular Dynamics simulations were performed using NAMD software package.[43] Timestep of 1 femtosecond was applied for each simulation. A cutoff of 14Å was applied for non-bonded interactions while Particle Mesh Ewald summation was applied for electrostatic interactions. The system was initially minimized for 200 steps. This was followed by equilibration at NVT ensemble. During this NVT equilibration the temperature was gradually raised from 5K to 315K with an increment of 10K. At each temperature 5000 steps (5 picoseconds) of simulation was performed. This was followed by 200 picoseconds of NVT equilibration at 300K. Thereafter the system was subjected to 400 picoseconds of equilibration at NPT ensemble. The temperature was kept fixed at 300K through Langevin dynamics with a damping coefficient of 5/ps while the pressure was controlled at 1 atm using Nose-Hoover Langevin piston. From the equilibrated system two initial production runs of each 10 nanoseconds were performed. The resultant snapshots were subjected to another two similar production run each. A final production run of 50 nanoseconds was performed from the final snapshot of the initial production run. The trajectory was stored for every 2 picoseconds. The trajectory from this final production run was used for calculation of all equilibrium properties. A similar protocol was followed for peptoid oligomers with alternating positive and negative φ dihedral angles.

ASSOCIATED CONTENT

Supporting Information

The Supporting Information regarding ^{1}H and ^{13}C NMR spectra for all compounds, 2D NOESY spectra for tetramers **6**, **12**, **19**, and **27**, the crystal structure report for dimer **17**, supporting Tables and Figures, Cartesian coordinates of optimized structures and fully detailed computational procedures is available free of charge on the ACS Publications website at DOI:

AUTHOR INFORMATION

Corresponding Authors

claude.taillefumier@univ-bpclermont.fr

lionel.perrin@univ-lyon1.fr

franck.jolibois@univ-tlse3.fr

Notes

The authors declare no competing financial interest.

CCDC 1824207 contains the supplementary crystallographic data for this paper. The data can be obtained free of charge from The Cambridge Crystallographic Data Centre via www.ccdc.cam.ac.uk/structures.

REFERENCES

(1) Guichard, G.; Huc, I. *Chem. Commun.* **2011**, *47*, 5933–5941.

(2) Gellman, S. H. *Acc. Chem. Res*. **1998**, 31, 173–180.

(3) Hill, D. J.; Mio, M. J.; Prince, R. B.; Hughes, T. S.; Moore, J. S. *Chem. Rev*. **2001**, 101, 3893–4012.

(4) a) Mándity, I. M.; Fülöp, F. *Expert Opin. Drug Discov.* **2015,** *10*, 1163–1177. b) Knight, A. S.; Zhou, E. Y.; Zuckermann, R. N. *Adv. Mater.* **2015,** *27*, 5665–5691.

(5) (a) Horne, W.; Gellman, S. H. *Acc. Chem. Res.* **2008,** *41*, 1399–1408. (b) Roy, A.; Prabhakaran, P.; Baruah, P. K.; Sanjayan, G. J. *Chem. Commun.* **2011,** *47*, 11593–11611. (c) Nair, R. V.; Vijayadas, K. N.; Roy, A.; Sanjayan, G. J. *Eur. J. Org. Chem.* **2014**, 7763–7780.

(6) Simon, R. J.; Kania, R. S.; Zuckermann, R. N.; Huebner, V. D.; Jewell, D. A.; Banville, S.; Ng, S.; Wang, L.; Rosenberg, S.; Marlowe, C. K.; Spellmeyer, D. C.; Tan, R.; Frankel, A. D.; Santi, D. V.; Cohen, F. E.; Bartlett, P. *Proc. Natl. Acad. Sci. USA* **1992**, *89*, 9367–9371.

(7) (a) Sui, Q.; Borchardt, D.; Rabenstein, D. L. *J. Am. Chem. Soc.* **2007,** *129*, 12042–12048. (b) Butterfoss, G. L.; Renfrew, P. D.; Kuhlman, B.; Kirshenbaum, K.; Bonneau, R. *J. Am. Chem. Soc.* **2009**, *131*, 16798–16807. (c) Voelz, V. A.; Dill, K. A.; Chorny, I. *Biopolymers* **2010**, *96*, 639-650. (d) Engel-Andreasen, J.; Wich, K.; Laursen, J. S.; Harris, P.; Olsen, C. A. *J. Org. Chem.* **2015**, *80*, 5415–5427.

(8) (a) Colapietro, M.; De Santis, P.; Palleschi, A.; Spagna, R. *Biopolymers*, **1986**, *25*, 2227–2236. (b) Benedetti, E.; Bavoso, A.; Di Blasio, B.; Pavone, V.; Pedone, C.; Toniolo, C.; Bonora, G. M. *Biopolymers*, **1983**, *22*, 305–317. (c) Mastle, W.; Dukor, R. K.; Yoder, G.; Keiderling, T. A. *Biopolymers*, **1995**, *36*, 623–631.

(9) Crisma, M.; Moretto, A.; Toniolo, C.; Kaczmarek, K.; Zabrocki, J. *Macromolecules* **2001**, *34*, 5048–5052.

(10) Crapster, J. A.; Guzei, I. A.; Blackwell, H. E. *Angew. Chem. Int. Ed.* **2013,** *52*, 5079–5084.

(11) Gorske, B. C.; Mumford, E. M.; Gerrity, C. G.; Ko, I. A. *J. Am. Chem. Soc.* **2017**, *139*, 8070-8073

(12) (a) Titlestad, K. A. *Acta Chem. Scand., Ser B*, **1975**, *29*, 153–167. (b) Groth, P. *Acta Chem Scand., Ser A*, **1970**, *24*, 780–790. (c) Maulucci, N.; Izzo, I.; Bifulco, G.; Aliberti, A.; De Cola, C.; Comegna, D.; Gaeta, C.; Napolitano, A.; Pizza, C.; Tedesco, C.; Flot, D.; De Riccardis, F. *Chem. Commun*. **2008**, 3927–3929. (d) Culf, A. S.; Cuperlovic-Culf, M.; Léger, D. A.; Decken, A. *Org. Lett*. **2014**, *16*, 2780–2783. (e) Tedesco, C.; Erra, L.; Izzo, I.; De Riccardis, F. *CrystEngComm* **2014**, *16*, 3667–3687.

(13) (a) Hjelmgaard, T.; Faure, S.; Caumes, C.; De Santis, E.; Edwards, A. A.; Taillefumier, C. *Org. Lett.* **2009,** *11*, 4100–4103. (b) Caumes, C.; Hjelmgaard, T.; Remuson, R.; Faure, S.; Taillefumier, C. *Synthesis* **2011,** 257–264. (c) De Santis, E.; Hjelmgaard, T.; Faure, S.; Roy, O.; Didierjean, C.; Alexander, B. D.; Siligardi, G.; Hussain, R.; Javorfi, T.; Edwards, A. A.; Taillefumier, C. *Amino Acids* **2011,** *41*, 663–672. (d) De Santis, E.; Hjelmgaard, T.; Caumes, C.; Faure, S.; Alexander, B. D.; Holder, S. J.; Siligardi, G.; Taillefumier, C.; Edwards, A. A. *Org. Biomol. Chem.* **2012,** *10*, 1108–1122. (e) Caumes, C.;

Fernandes, C.; Roy, O.; Hjelmgaard, T.; Wenger, E.; Didierjean, C.; Taillefumier, C.; Faure, S. *Org. Lett.* **2013**, *15*, 3626–3629.

(14) Roy, O.; Caumes, C.; Esvan, Y.; Didierjean, C.; Faure, S.; Taillefumier, C. *Org. Lett.* **2013**, *15*, 2246–2249.

(15) (a) Armand, P.; Kirshenbaum, K.; Falicov, A.; Dunbrack Jr, R. L.; Dill, K. A.; Zuckermann, R. N.; Cohen, F. E. *Fold. Des.* **1997,** *2*, 369–375. (b) Wu, C. W.; Kirshenbaum, K.; Sanborn, T. J.; Patch, J. A.; Huang, K.; Dill, K. A.; Zuckermann, R. N.; Barron, A. E. *J. Am. Chem. Soc.* **2003**, *125*, 13525–13530. (c) Wu, C. W.; Sanborn, T. J.; Huang, K.; Zuckermann, R. N.; Barron, A. E. *J. Am. Chem. Soc.* **2001**, *123*, 6778–6784. (d) Stringer, J. R.; Crapster, J. A.; Guzei, I. A.; Blackwell, H. E. *J. Am. Chem. Soc.* **2011**, *133*, 15559–15567. (e) Roy, O.; Dumonteil, G.; Faure, S.; Jouffret, L.; Kriznik, A.; Taillefumier, C. *J. Am. Chem. Soc.* **2017**, *139*, 13533–13540.

(16) (a) Shah, N. H.; Butterfoss, G. L.; Nguyen, K.; Yoo, B.; Bonneau, R.; Rabenstein, D. L.; Kirshenbaum, K. *J. Am. Chem. Soc*. **2008**, *130*, 16622–16632. (b) Stringer, J. R.; Crapster, J. A.; Guzei, I. A.; Blackwell, H. E. *J. Org. Chem.* **2010**, *75*, 6068–6078.

(17) (a) Caumes, C.; Roy, O.; Faure, S.; Taillefumier, C. *J. Am. Chem. Soc.* **2012,** *134*, 9553–9556. (b) Aliouat, H.; Caumes, C.; Roy, O.; Zouikri, M.; Taillefumier, C.; Faure, S. *J. Org. Chem.* **2017,** *82*, 2386–2398.

(18) Angelici, G.; Bhattacharjee, N.; Roy, O.; Faure, S.; Didierjean, C.; Jouffret, L.; Jolibois, F.; Perrin, L.; Taillefumier, C. *Chem. Commun.* **2016**, *52*, 4573–4576.

(19) (a) Zuckermann, R. N.; Kerr, J. M.; Kent, S. B. H.; Moos, W. H. *J. Am. Chem. Soc.* **1992**, *114*, 10646–10647. (b) Culf, A. S.; Ouellette, R. J. *Molecules* **2010**, *15*, 5282–5335.

(20) Hamper, B. C.; Kolodziej, S. A.; Scates, A. M.; Smith, R. G.; Cortez, E. *J. Org. Chem* **1998**, *63*, 708–718.

(21) De K.; Legros J.; Crousse B.; Bonnet-Delpon D. *J. Org. Chem*. **2009**, *74*, 6260–6265.

(22) Matsugi, M.; Suganuma, M.; Yoshida, S.; Hasebe, S.; Kunda, Y.; Hagihara, K.; Oka, S.; *Tetrahedron Lett*. **2008**, *49*, 6573–6574.

(23) Laursen, J. S.; Engel-Andreasen, J.; Fristrup, P.; Harris, P.; Olsen, C. A. *J. Am. Chem. Soc.* **2013**, *135*, 2835–2844.

(24) Hinderaker, M. P.; Raines, R. T. *Protein Science*, **2003**, *12*, 1188–1194.

(25) Newberry, R. W.; VanVeller, B.; Guzei, I. A.; Raines, R. T. *J. Am. Chem. Soc.* **2013**, *135*, 7843–7846.

(26) Gorske, B. C.; Bastian, B. L.; Geske, G. D.; Blackwell, H. E. *J. Am. Chem. Soc.* **2007**, *129*, 8928–8929.

(27) (a) Becke, A. B. *J. Chem. Phys.* **1993**, *98*, 5648–5652. (b) Lee, C.; Yang, W.; Parr, R. G. *Phys. Rev. B* **1988**, *37*, 785–789.

(28) Foresman, A. E., in *Exploring chemistry with electronic structure methods*, Gaussian Inc., Pittsburgh, 2nd edn., **1998**.

(29) (a) Wolinski, K.; Sadlej, A. J. *Mol. Phys.* **1980**, *41*, 1419–1430. (b) Wolinski, K.; Hinton, J. F.; Pulay, P. *J. Am. Chem. Soc,* **1990**, *112*, 8251–8260. (c) London, F. J. *J. Phys. Radium* **1937**, *8*, 397–409. (d) McWeeny, R. *Phys. Rev.* **1962**, *126*, 1028–1034. (e) Ditchfield, R. *Mol. Phys.* **1974**, *27*, 789–807. (f) Dodds, J. L.; McWeeny, R.; Sadlej, A. J. *Mol. Phys.* **1977**, *34*, 1779–1791.

(30) Jolibois, F.; Soubias, O.; Réat, V.; Milon, A. Chemistry. *Eur.–J.* **2004**, *10*, 5996–6004.

(31) Laursen, J. S.; Harris, P.; Fristrup, P.; Olsen, C. A. *Nat. Commun.* **2015**, *6*, 7013-7023

(32) Zuliani, V.; Carmi, C.; Rivara, M.; Fantini, M.; Lodola, A.; Vacondio, F; Bordi, F Plazzi, P. V.; Cavazzoni, A.; Galetti, M.; Alfieri, R. R.; Petronini, P. G.; Mor, M. *Eur. J. Med. Chem*. **2009**, *44*, 3471–3479.

(33) Muralirajan, K.; Haridharan, R.; Prakash, S.; Cheng, C.-H. *Adv. Synth. Catal.* **2015**, *357,* 761–766.

(34) GaussView, Version 5, Roy Dennington, Todd Keith, and John Millam, Semichem Inc., Shawnee Mission, KS, 2009.

(35) Gaussian 09, Revision D.01, Frisch, M. J.; Trucks, G. W.; Schlegel, H. B.; Scuseria, G. E.; Robb, M. A.; Cheeseman, J. R.; Scalmani, G.; Barone, V.; Mennucci, B.; Petersson, G. A.; Nakatsuji, H.; Caricato, M.; Li, X.; Hratchian, H. P.; Izmaylov, A. F.; Bloino, J.; Zheng, G.; Sonnenberg, J. L.; Hada, M.; Ehara, M.; Toyota, K.; Fukuda, R.; Hasegawa, J.; Ishida, M.; Nakajima, T.; Honda, Y.; Kitao, O.; Nakai, H.; Vreven, T.; Montgomery, Jr., J. A.; Peralta, J. E.; Ogliaro, F.; Bearpark, M.; Heyd, J. J.; Brothers, E.; Kudin, K. N.; Staroverov, V. N.; Kobayashi, R.; Normand, J.; Raghavachari, K.; Rendell, A.; Burant, J. C.; Iyengar, S. S.; Tomasi, J.; Cossi, M.; Rega, N.; Millam, J. M.; Klene, M.; Knox, J. E.; Cross, J. B.; Bakken, V.; Adamo, C.; Jaramillo, J.; Gomperts, R.; Stratmann, R. E.; Yazyev, O.; Austin, A. J.; Cammi, R.; Pomelli, C.; Ochterski, J. W.; Martin, R. L.; Morokuma, K.; Zakrzewski, V. G.; Voth, G. A.; Salvador, P.; Dannenberg, J. J.; Dapprich, S.; Daniels, A. D.; Farkas, Ö.; Foresman, J. B.; Ortiz, J. V.; Cioslowski, J.; Fox, D. J. Gaussian, Inc., Wallingford CT, 2009.

(36) Zhao, Y.; Truhlar, D. G. *Theor. Chem. Acc.* **2008**, *120*, 215–241.

(37) (a) McLean, A. D.; Chandler, G. S. *J. Chem. Phys.* **1980**, *72*, 5639–5648. (b) Raghavachari, K.; Binkley, J. S.; Seeger, R.; Pople J. A. *J. Chem. Phys.* **1980**, *72*, 650–654.

(38) Marenich, A. V.; Cramer, C. J.; Truhlar, D. G. *J. Phys. Chem. B* **2009**, *113*, 6378–6396.

(39) Schaefer, A.; Horn, H.; Ahlrichs, R. *J. Chem. Phys.* **1992**, *97*, 2571–2577.

(40) Wang, J.; Wolf, R. M.; Caldwell, J. W.; Kollman, P. A.; Case, D. A. *J. Comput. Chem.* **2004**, *25*, 1157–1174.

(41) Vanquelef, E.; Simon, S.; Marquant, G.; Garcia, E.; Klimerak, G.; Delepine, J. C.; Cieplak, P.; Dupradeau, F. *Nucl. Acids Res.* **2011**, 1-7.

(42) Wang, J.; Wang, W.; Kollman P. A.; Case, D. A. *J. Mol. Graph. Model.* **2006**, *25*, 247–260.

(43) Phillips, J. C.; Braun, R.; Wang, W.; Gumbart, J.; Tajkhorshid, E.; Villa, E.; Chipot, C.; Skeel, R. D.; Kale, L.; Schulten, K. *J. Comp. Chem.* **2005**, *26*, 1781–1802.